Mechanical Systems and Signal Processing 70-71 (2016) 578–600

A spectrum-driven damage identification technique: Application and validation through the numerical simulation of the Z24 Bridge

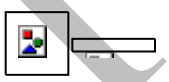

Maria-Giovanna Masciotta [a,n], Luís F. Ramos [a], Paulo B. Lourenço [a], Marcello Vasta [b], Guido De Roeck [c]

[a] University of Minho, Department of Civil Engineering, Campus de Azurém, 4800-058 Guimarães, Portugal
[b] University "G.d'Annunzio", Department of Engineering and Geology, 65127 Pescara, Italy
[c] Catholic University of Leuven, Department of Civil Engineering, Kasteelpark Arenberg 40, B-3001 Leuven, Belgium

a r t i c l e i n f o

Article history:
Received 27 June 2014
Received in revised form
13 August 2015
Accepted 27 August 2015
Available online 29 September 2015

Keywords:
Damage identification
Spectrum-driven method
Damage localization index
Power spectral densities
Concrete bridges

a b s t r a c t

The present paper focuses on a damage identification method based on the use of the second order spectral properties of the nodal response processes. The explicit dependence on the frequency content of the outputs power spectral densities makes them suitable for damage detection and localization. The well-known case study of the Z24 Bridge in Switzerland is chosen to apply and further investigate this technique with the aim of validating its reliability. Numerical simulations of the dynamic response of the structure subjected to different types of excitation are carried out to assess the variability of the spectrum-driven method with respect to both type and position of the excitation sources. The simulated data obtained from random vibrations, impulse, ramp and shaking forces, allowed to build the power spectrum matrix from which the main eigenparameters of reference and damage scenarios are extracted. Afterwards, complex eigenvectors and real eigenvalues are properly weighed and combined and a damage index based on the difference between spectral modes is computed to pinpoint the damage. Finally, a group of vibration-based damage identification methods are selected from the literature to compare the results obtained and to evaluate the performance of the spectral index.

1. Introduction

Research activities in vibration-based damage identification methods (VBDIMs) have been increasing more and more within the engineering community over the last decades. The possibility of catching the occurrence of damage at the earliest stage by means of global non-invasive tools is the drive behind this trend. Conventional non-destructive techniques (NDT), such as computed tomography, laser scanning, ultrasonic and acoustic methods, are approaches mostly suitable for detecting local damage. When dealing with large and complicated structures in invisible or closed environments, the

[n] Correspondence to: University of "G.d'Annunzio", Department of Engineering and Geology, Viale Pindaro, 65127 Pescara, Italy. Mobile: þ 351 917099832, þ39 3381238998.
E-mail addresses: mg.masciotta@gmail.com (M.-G. Masciotta), lramos@civil.uminho.pt (L.F. Ramos), pbl@civil.uminho.pt (P.B. Lourenço), mvasta@unich.it (M. Vasta), guido.deroeck@bwk.kuleuven.be (G. De Roeck).

http://dx.doi.org/10.1016/j.ymssp.2015.08.027

applicability of these techniques becomes very difficult [1]. Hence referring to dynamic-based methods as a global way to assess the structural condition of non-conventional systems becomes necessary.

Considering the explicit dependence of the modal parameters on the physical properties of the structure and vice versa, several methods have been addressed to damage detection and localization using changes in system dynamic characteristics [2]. Most of the emphasis has been put on the use of frequency losses as 'damage indicator', but the frequencies alone cannot provide spatial information about structural damage since they refer to global parameters, whereas damage is a local phenomenon that can yield the same amount of frequency change even if associated with different locations. Furthermore, the sensitivity to mass variation and environmental conditions introduces uncertainties in the measured frequencies [3,4], revealing their limited feasibility for the purpose of damage localization. Due to that, the focus of the research activity has turned towards more sensitive modal parameters, such as mode shapes and modal curvatures [5], which dependence on the nodal coordinates of the system makes them appropriate for locating the damage. However, exciting higher modes from vibration tests in order to capture local changes is not always feasible, especially in case of large and heavy structures. This fact, coupled with the loss of information due to the inevitable reduction of time-history measurements, can affect the outcome of the damage investigation procedure. Other approaches in detecting and locating the damage have been either the use of changes in structural parameters, such as stiffness and flexibility [6–8], or 'model-based approaches' like the FE model Updating [9], a method based on a sensitivity formulation aimed at selecting the most suitable parameters to be updated in order to minimize the difference between numerical and experimental responses and to identify the location of the damage. One of the major drawback in this case is the lack of measured degrees-of-freedom (DOFs) with respect to the analytical ones. Modern-type vibration-based approaches have also been addressed, i.e. methods based on wavelet analysis, neural network or genetic algorithm [1], but their efficiency in detecting damage must be further validate. It needs to remark that the identification of structural damage at the earliest possible stage is very important in all the engineering fields, since it allows to keep under control and assess the structural conditions, to manage the potential seismic risk of structures and to plan efficient repair works before the accumulation of damage over time becomes an irreversible condition. All above mentioned reasons clearly explain why VBDIMs are techniques still under development.

The methodology here presented investigates the second order spectral properties of nodal response processes with the purpose of defining a spectrum-driven method able to detect and localize the structural damage by means of a proper combination of the eigenparameters, namely eigenvalues and eigenvectors, extracted from the output Power Spectral Density (PSD) matrix. Appealing features of this method are: (1) the possibility of identifying the modal parameters using exclusively the acceleration time-histories of selected points, collected either from output-only or input–output techniques; (2) the capacity of identifying closely spaced modes; (3) the advantage of ranging over the whole frequency domain, without reducing the damage investigation procedure to a limited number of resonant frequencies; and (4) the possibility of catching the occurrence of damage even if not visible to human eyes. The theoretical background on which the proposed approach lies is concisely presented in the first part of the paper, while the second part of the work focuses on the application of this method to a numerical model simulating a pre-stressed concrete bridge, the Z24. Before being destroyed and replaced by a new one, in the framework of the Brite Euram project BE 96-3157 SIMCES (System Identification to Monitor Civil Engineering Structures), progressive damage tests were carried out to study the dynamic response of the bridge, located in Switzerland. Detailed information about the experimental campaign can be found in [10] and [40]. The selection of this well-known case study has been driven by the necessity of having a full-scale benchmark in order to analyze and validate the spectral method hereafter introduced. In detail, the next sections of the present paper are organized as follows: Section 2 presents a concise review of the most representative algorithm-based damage identification methods available in the literature, Section 3 deals with the theoretical aspects of the method and the definition of the spectral index; Section 4 presents the dynamic analyses performed on the case-study with the purpose of validating the spectral approach; Section 5 discusses the obtained results; Section 6 is dedicated to the comparison of the spectral damage index with a group of well-known damage indexes selected from the literature; and Section 7 summarizes the most important points of the work and presents the final conclusions that can be derived from the proposed method.

Based on the work presented by [11], new aspects are addressed in the present work. Besides a more scientifically detailed description of the theoretical framework necessary for a thorough understanding of the proposed formulation, the numerical damage simulation of the bridge has been reformulated and an in-depth study on the sensitivity of the spectral damage localization index with regard to both type and spatial distribution of the input force has been carried out as well. Additionally, the spectral results have been compared to the ones obtained from other vibration-based damage identification methods with the purpose of weighing the performance of the introduced approach. Finally, the paper has been enriched with the study of the influence of the number of DOFs on the outcome of the spectral damage analysis.

2. State of the art

The field of damage identification is very broad and encompasses several methods categorized depending on various criteria. Vibration-based damage identification methods (VBDIMs) supported by continuous structural health monitoring are probably the best tool available to evaluate the structural conditions and to catch the onset of damage at the earliest possible stage, especially when dealing with non-conventional systems. Such methods can be classified according to the effect of the damage on the structure or to the level of identification attempted. With respect to the effect of damage,

VBDIMs can be sorted in linear and non-linear, depending on the behavior that characterizes the structure after the occurrence of damage. Linear methods can be further distinguished in modal-based and non-modal-based, depending on whether or not changes in modal parameters are used to infer the damage. Modal-based methods can be then sorted in model-based and non-model-based methods. The former group differs from the latter for the recourse during the damage analysis to a discretized FE model representative of the system response.

With respect to the level of identification, VBDIMs can be classified according to the following hierarchical levels [12]:

- Level 1 (Detection) – the method gives qualitative indication about the occurrence of damage in the structure;
- Level 2 (Localization) – the method provides spatial information about the possible damage location;
- Level 3 (Assessment) – the method gives an estimate of the size of the damage;
- Level 4 (Prediction) – the method offers information about the actual safety of the structure, estimating the remaining service life.

The classification above has been recently extended by the introduction of a new level (Classification) as intermediate step between Localization and Assessment, see [13,14,1]. Methods providing information about the type of damage belong to this level. For convenience, hereafter the four-level classification will be referred to.

The approach proposed in this study belongs to the category of modal-based methods and investigates three levels of identification: damage detection, damage localization and damage assessment. It is stressed that the third level of identification is here treated only from a qualitative point of view. The relationship between qualitative and quantitative damage measures has not been addressed. As a global non-destructive dynamic-based technique, the spectrum-driven method exploits the second order moments (or power spectral densities) of the vibration characteristics of structures to identify the damage. This technique is based upon the diagonalization of the spectral density matrix which has been in use since the early 1980s to obtain the modes of a vibrating system subjected to natural excitation [15]. Afterward, it has been applied to FRFs becoming known as the Complex Mode Indication Function (CMIF) [16], tool used to count the number of modes present in the measurement data. Higher order spectral methods for structural identification have also been developed [17,18]. In the last decades the use of power spectral densities has been extended to the field of damage identification. Liberatore et al. [19,20] used the Power Spectral Density (PSD) approach to locate the damage in a simply supported beam by using the energy localized in bandwidth regions $[\omega_1, \omega_2]$ near resonance since they are more sensitive to damage. For each region, the energy is estimated by Power Spectral Density analysis and quantified by means of the Root Mean Square (RMS) of its transfer function $H(\omega)$ as:

$$\mathrm{RMS} = \sqrt{\frac{1}{2\pi}\int_{\omega_1}^{\omega_2} |H(\omega)|^2 d\omega} \tag{1}$$

A damage localization index (DLM) based on the comparison between RMS values obtained from undamaged and damaged conditions is then defined to infer the damage in the structure:

$$\mathrm{DLM} = \sum_{i=1}^{N} \left| \frac{(\mathrm{RMS}_i)_U - (\mathrm{RMS}_i)_D}{(\mathrm{RMS}_i)_U} \right| \tag{2}$$

As this index cannot go beyond level 1 damage identification, in order to pinpoint the damage, the authors defined a Damage Localization function DL(x) by introducing a modal parameter in the formulation:

$$\mathrm{DL}(x) = \sum_{i=1}^{N} \left| \frac{(\mathrm{RMS}_i)_U - (\mathrm{RMS}_i)_D}{(\mathrm{RMS}_i)_U} \right| \cdot |\varphi_i(x)| \tag{3}$$

where the function $\varphi(x)$ is the absolute value of the ith mode shape of the undamaged structure and N is the number of mode shapes.

In [21] a spectral-based hierarchical damage detection algorithm for smart sensor networks is examined. The approach is an extension of a previous work that studied the changes in the Power Spectral Density (PSD) of structures induced by damage. Using the normalized direct PSDs of output measurements $P_i(f) = S_{ii}(f) / \sqrt{\sum_{j=1}^{n} S_{ii}(f)^2}$ and the corresponding normalized PSDs curvatures $P''_{ii}(f) = S''_{ii}(f) / \sqrt{\sum_{j=1}^{n} S''_{ii}(f)^2}$, two damage indicators are defined, viz. the Absolute Difference PSD (ADPSD) Method and the Curvature Difference PSD (CDPSD) Method:

$$\Delta P_i(f) = \left| P_i^u(f) - P_i^d(f) \right| \qquad \Delta P''_i(f) = \left| P''^u_i(f) - P''^d_i(f) \right| \tag{4}$$

Either indicator in Eq. (4) is used to compute an Accumulated Damage Index (ADI) in order to detect and locate the damage. Applied to the FE model of a planar truss, the modified algorithm results effective in damage detection and location when limitations of node overlap, cluster size, cut-off frequency are properly observed. However, further research is recommended to expand these results and overcome the identified limitations.

Two spectral-based damage localization indexes have also been proposed by Fang and Perera [22]: the Power Mode Shape Curvature (PMSC) and the Power Flexibility (PF). Basic parameters in either index are the Power Mode Shape (PMS)

vectors ψ_i obtained directly from bandwidth-localized PSDs of the output signals without any modal analysis:

$$\psi_i = \left\{ \int_{\omega_1}^{\omega_2} S_{ii}(\omega) d\omega \right\}^{1/2} \tag{5}$$

Once the PMSs are estimated, the corresponding PMSCs can be calculated at each measurement point by the central finite difference theorem. The largest absolute difference between the PMSC vectors of undamaged Υ_i^u and damaged Υ_i^d structure will target the damage position:

$$\Delta\Upsilon_i = \left| \Upsilon_i^u - \Upsilon_i^d \right| \tag{6}$$

The method is first applied to a single-span beam and then to an 8-dof mass–spring system, revealing some deficiency for the damage localization. Thus, to improve the results, the authors define another index based on the change of PFs before and after damage, as follows:

$$\Delta\mathbf{F} = \breve{\mathbf{F}}_d - \breve{\mathbf{F}}_u \tag{7}$$

Unlike conventional flexibility, which is defined by physical quantities, for its definition power flexibility employs both statistical parameters of vibration signals and modal frequencies:

$$\breve{\mathbf{F}} = \breve{\boldsymbol{\Phi}}\breve{\boldsymbol{\Lambda}}^{-1}\boldsymbol{\Phi}^T \text{ with diagonal elements of } \sum_{j=1}^{m} \frac{(\psi_{i,j})^2}{\omega_j^2} \tag{8}$$

where $\mathbf{F}$ denotes the PF matrix, $\boldsymbol{\Phi}$ denotes the PMS matrix consisting of m fundamental power modes ψ_i and $\boldsymbol{\Lambda}$ is the eigenvalue square matrix consisting of circular frequency ω_j in rad/s or modal frequency f in Hz. The introduction of modal parameters in the PF index enables to obtain better results, although more general conclusions would require further studies.

In [23] two spectral-based non-parametric damage detection methods are applied to a set of composite beams. The first is based on the Power Spectral Density (PSD) of a single response, and the second on the Transmittance Function (TF) between two responses. According to that, the following damage indexes are defined:

$$F = \frac{\hat{S}_o(\omega)/S_o(\omega)}{\hat{S}_u(\omega)/S_u(\omega)} \qquad D = \frac{\left|\hat{T}_o(i\omega)\right|}{\left|\hat{T}_u(\omega)\right|} \tag{9}$$

in which $S_o(\omega)$ and $S_u(\omega)$ are the unknown PSDs of healthy and current structural response, respectively, $\hat{S}_o(\omega)$and $\hat{S}_u(\omega)$ are their estimates, whereas $\hat{T}_o(\omega)$ and $\hat{T}_u(\omega)$ are the Welch-based estimates of the unknown TFs, namely $T_o(\omega)$ and $T_u(\omega)$, of healthy and current states of the structure, computed as follows:

$$T_{lm}(i\omega) = \frac{S_{ml}(i\omega)}{S_{ll}(\omega)} \tag{10}$$

where the subscripts l, m designate two measurement points on the structure, S_{ml} is the cross PSD between signals at points l and m, and S_{ll} is the PSD of the signal at point l. For both indexes, the results have shown the problem of degraded detection performance caused by material and manufacturing variability among the beams.

2.1. Traditional modal-based damage identification methods

Commonly used method to compare two sets of mode shapes belonging to different scenarios, i.e. undamaged and damaged state, is the Coordinate Modal Assurance Criterion (COMAC) [31], an extension of the Modal Assurance Criterion (MAC). The COMAC value is a point-wise measure ranging between zero and one, and it can be computed for each measurement point i (DOF) through the following expression:

$$\mathrm{COMAC}_{i,u,d} = \frac{\left|\sum_{j=1}^{m} \varphi_{i,j}^u \varphi_{i,j}^d\right|^2}{\sum_{j=1}^{m} (\varphi_{i,j}^u)^2 \sum_{j=1}^{m} (\varphi_{i,j}^d)^2} \tag{11}$$

where φ_u and φ_d are the mode shape vectors of undamaged and damaged conditions and m is the number of estimated mode shapes. Values near zero indicate discordance at a certain point and this might imply a possible damage location.

The Parameter Method (PM) proposed by Dong et al. [32] is based on the combination of mode shapes and resonant frequencies as follows:

$$\Delta\phi = \sum_{j=1}^{m} \left[\left| \phi_j^d \right| \left(\frac{1}{\omega_j^d} - \frac{1}{\omega_j^u} \right) \right] \tag{12}$$

where the ratio between the frequencies characterizing undamaged and damaged scenarios is inversely proportional to the damage size. An equivalent and more sensitive parameter is computed using the strain mode shapes instead of displacements.

Pandey et al. [5] defined a technique known as Mode Shape Curvature Method (MSCM) which is based on the absolute difference in the modal curvatures φ_j'' between the sound and the damaged configurations:

$$\Delta\varphi'' = \sum_{j=1}^{m} \left| \varphi_{d,j}'' - \varphi_{u,j}'' \right| \tag{13}$$

As a tentative to improve the results, the Sum of all Curvatures Errors (SCE) is introduced:

$$\mathrm{SCE} = \sum_{j=1}^{m} \left| \frac{\left(\varphi_{d,j}'' - \varphi_{u,j}'' \right)}{\varphi_{u,j}''} \right| \tag{14}$$

Stubbs et al. [33] presented a Damage Index Method (DIM) for beam-like structures based on the decrease in modal strain energy between two measurement points a and b at locations i and $i+1$, respectively. The index is given by the expression:

$$\beta_{i,j} = \frac{\left[\int_a^b (\varphi_j^{d''})^2 dx + \int_0^L (\varphi_j^{d''})^2 dx \right] \cdot \left[\int_a^b (\varphi_j^{u''})^2 dx + \int_0^L (\varphi_j^{u''})^2 dx \right]}{\left[\int_a^b (\varphi_j^{d''})^2 dx + \int_0^L (\varphi_j^{d''})^2 dx \right] \cdot \left[\int_a^b (\varphi_j^{u''})^2 dx + \int_0^L (\varphi_j^{u''})^2 dx \right]} \tag{15}$$

where $\varphi_j^{d''}(x)$ and $\varphi_j^{u''}(x)$ are the modal curvatures of the jth mode shape in the damaged and undamaged condition and L is the length of the structure. The damage index of the ith segment is then given by taking into account the contribution of all the modes, as follows:

$$\beta_i = \sum_{j=1}^{m} \beta_{i,j} \tag{16}$$

Finally, assuming that the damage index β at different sub-regions is a normally distributed random variable, the possible damage locations are estimated from the normalized index Z_i where $\bar{\beta}_i$ and s_i are the mean value and the standard deviation of the damage indexes:

$$Z_i = (\beta_i - \bar{\beta}_i)/\sigma_i \tag{17}$$

Values with a magnitude greater than two indicate members that are likely damaged.

Pandey and Biswas [6] suggested and demonstrated the use of the Change in Flexibility Matrix (CFM) in detecting and locating the damage in a wide-flange steel beam. Given two sets of measurements, one for the intact structure and another for the damaged structure, the CFM is given by:

$$\beta = diag\left\{ \mathbf{F}^d - \mathbf{F}^u \right\} \tag{18}$$

where F is the dynamically flexibility matrix estimated from mass-normalized measured mode shapes ϕ_j and corresponding frequencies ω_j:

$$\mathbf{F} = \mathbf{\Phi}_m \mathbf{\Lambda}_m^{-1} \mathbf{\Phi}_m^T = \sum_{j=1}^{m} \frac{1}{\omega_j^2} \phi_j \phi_j^T \tag{19}$$

Because of the inverse relationship to the square of the modal frequencies, the flexibility matrix is most sensitive to changes in the lower frequency modes, which can be easily extracted in the real practice by means of output-only techniques.

2.2. *Proposed approach for damage identification*

Despite the employment of power spectral densities for damage identification purposes is not completely new in the literature, in the present paper their use has been reformulated according to a novel concept of spectral modes and leading to the definition of a new damage localization index which inherently takes into account the contribution of both direct and cross-modal terms to PSDs. It is important to stress that if the damping in the system is small and the modal frequencies are well separated, then the contributions of cross-modal terms to auto spectral densities are smaller than the contributions

from single modes given by direct-modal terms [24]. But if these conditions are not verified, the consideration of cross-modal terms is necessary. Since eigenvalues and eigenvectors already contain the cross-modal terms contributions, it follows that the analysis of the system's response PSD matrix through its eigenvalue decomposition can lead to more accurate results in terms of damage identification with respect to the analysis of single PSDs estimates. Moreover, the addressed spectral index is conceived to range over the whole frequency domain allowing to consider the entire energy distribution of each vibration mode in the spectral damage analysis.

Beyond the numerical validation, the performance of the proposed approach will be weighed and evaluated through the comparison of the spectral results with the ones obtained from other VBDIMs. A review of all techniques developed hitherto falls outside the scope of the present paper and the reader is referred to [25–28] for this purpose. Here, only a group of methods is selected for the comparison, viz.: Co-ordinate Modal Assurance Criterion (COMAC); Parameter Method (PM); Mode Shape Curvature Method (MSCM); Sum of all Curvature Errors method (SCE); Damage Index Method (DIM); Changes in Flexibility Matrix method (CFM). All chosen techniques belong to the category of traditional modal-based methods and require similar modal quantities to identify the damage. Hereafter, each technique is briefly presented. A detailed description can be found elsewhere [29,30].

3. The spectral-based damage identification method

The stochastic loadings experienced by a structure during its lifespan are essentially uncertain in nature and must be defined in a statistical sense, by adopting stochastic models expressed in terms of random processes. In this context, the response X(t) of a system to a dynamic loading F(t) is defined as unidimensional multivariate stochastic process since it includes all system's nodal response processes, which depend on the same deterministic parameter, namely time. In the frequency domain, the characterization of stochastic processes requires the evaluation of the *spectral density* functions, defined according to the Wiener–Khintchine relationships as the Fourier Transforms of the corresponding time-domain correlation functions. For continuous time signals, the aforementioned relationships are given by the following expressions:

$$S_X(\omega) = \frac{1}{2\pi}\int_{-\infty}^{+\infty} R_X(\tau)\, e^{-i\omega\tau} d\tau, \qquad S_Y(\omega) = \frac{1}{2\pi}\int_{-\infty}^{+\infty} R_Y(\tau)\, e^{-i\omega\tau} d\tau, \qquad S_{XY}(\omega) = \frac{1}{2\pi}\int_{-\infty}^{+\infty} R_{XY}(\tau)\, e^{-i\omega\tau} d\tau \tag{20}$$

where $R_X(\tau)$ and $R_Y(\tau)$ are the auto correlation functions of the processes $X(t)$ and $Y(t)$, respectively, while $R_{XY}(\tau)$ is the related cross correlation function. From Eq. (20) it is possible to infer that the spectral density function is a complete frequency decomposition of a stationary correlation function, providing information about the average energy distribution of a random process over the frequency domain.

In real situations, one deals with discrete time signals ranging over a finite time interval. As a consequence of that, it needs to compute the Discrete Fourier Transform (DFT) of the process, equivalent of the continuous Fourier Transform for signals known only at N instants separated by sample times $T = N\Delta t$:

$$X(\omega_l, T) = \int_0^T x(t) e^{-i\omega_l t} dt = \sum_{k=1}^{N} x(k\Delta t) e^{-i\omega_l k\Delta t} \Delta t \tag{21}$$

having set $\omega_l = l\frac{2\pi}{N\Delta t}$ rad/s with $l = 0, 1, \ldots, n$.

Thus, given two discrete stochastic processes $X(t)$ and $Y(t)$, the corresponding spectral quantities or second moment functions must be written in the form:

$$\begin{aligned} S_X(\omega_n, T) &= \frac{E[X(\omega_n, T) X(\omega_n, T)^*]}{2\pi T} = \frac{\sum_{j=1}^{N}\sum_{k=1}^{N} x(j\Delta t) x(k\Delta t) e^{-i\omega_n (j-k)\Delta t}\Delta t}{2\pi N n_s} \\ S_Y(\omega_n, T) &= \frac{E[Y(\omega_n, T) Y(\omega_n, T)^*]}{2\pi T} = \frac{\sum_{j=1}^{N}\sum_{k=1}^{N} y(j\Delta t) y(k\Delta t) e^{-i\omega_n (j-k)\Delta t}\Delta t}{2\pi N n_s} \\ S_{XY}(\omega_n, T) &= \frac{E[X(\omega_n, T) Y(\omega_n, T)^*]}{2\pi T} = \frac{\sum_{j=1}^{N}\sum_{k=1}^{N} x(j\Delta t) y(k\Delta t) e^{-i\omega_n (j-k)\Delta t}\Delta t}{2\pi N n_s} \end{aligned} \tag{22}$$

where $E[\bullet]$ means ensemble average, n_s represents the number of registrations, while $X(\omega,T)^*$ and $Y(\omega,T)^*$ are the complex conjugates of the processes $X(\omega,T)$ and $Y(\omega,T)$, respectively.

3.1. Power Spectrum Matrix

The spectral density functions can be collected in in the frequency-domain counterpart of the correlation matrix, namely the Power Spectral Density (PSD) matrix. In the simplest case of bivariate unidimensional stationary stochastic process this matrix equals:

$$\mathbf{S}_X(\omega, T) = \frac{1}{2\pi}\int_0^T \mathbf{R}_X(\tau)\, e^{-i\omega\tau} d\tau = \begin{bmatrix} S_X(\omega, T) & S_{XY}(\omega, T) \\ S_{YX}(\omega, T) & S_Y(\omega, T) \end{bmatrix} \tag{23}$$

where diagonal and out-of-diagonal elements represent the direct and cross power spectral densities of the processes $X(\omega,T)$ and $Y(\omega,T)$, respectively. Since direct spectral densities $S_X(\omega,T)$ and $S_Y(\omega,T)$, or auto-spectra, are real functions while cross spectral densities, or cross-spectra, are complex conjugate functions, i.e. $\mathbf{S}_{XY}(\omega, T) = \mathbf{S}^*_{YX}(\omega, T)$ due to the circumstance $R_{YX}(\tau) = R_{XY}(-\tau)$, it follows that the matrix in Eq. (23) is a Hermitian matrix consisting of a symmetric real part and an anti-symmetric imaginary part:

$$\mathbf{S}_X(\omega, T) = \begin{bmatrix} S_X(\omega, T) & \mathrm{Re}\{S_{XY}(\omega, T)\} \\ \mathrm{Re}\{S_{XY}(\omega, T)\} & S_Y(\omega, T) \end{bmatrix} + i \begin{bmatrix} 0 & \mathrm{Im}\{S_{XY}(\omega, T)\} \\ -\mathrm{Im}\{S_{XY}(\omega, T)\} & 0 \end{bmatrix} \tag{24}$$

The relations so far addressed can be easily extended to the case of multivariate stochastic process, by increasing the order of the PSD matrix according to the number m of measured nodal response processes as follows:

$$\mathbf{S}_X(\omega, T) = \begin{bmatrix} S_{X_1X_1}(\omega, T) & S_{X_1X_2}(\omega, T) & \cdots & S_{X_1X_m}(\omega, T) \\ \cdots & \cdots & \cdots & \cdots \\ S_{X_mX_1}(\omega, T) & \cdots & \cdots & S_{X_mX_m}(\omega, T) \end{bmatrix} \tag{25}$$

Since Hermitian, see Eq. (24), the Power Spectral Density matrix $S_X(\omega,T)$ admits real positive-defined eigenvalues $\lambda_i(\omega)$ and complex eigenvectors $\psi_i(\omega)$. Note that an m-by-m matrix will have m eigenvalues and m eigenvectors. As eigenvalues are quantities sensitive to changes in the matrix elements, the properties of the PSD matrix can be analyzed through its eigenvalue decomposition:

$$\mathbf{S}_X(\omega) = \mathbf{\Psi}_X(\omega)\mathbf{\Lambda}_X(\omega)\mathbf{\Psi}^H_X(\omega) \tag{26}$$

in which $\Lambda_x(\omega) = diag\{\lambda_1, \lambda_2, \ldots, \lambda_j, \ldots, \lambda_m\}$ is a diagonal matrix containing frequency-dependent nonnegative eigenvalues in decreasing order and $\Psi_x(\omega) = [\psi_1\ \psi_2\ \ldots\ \psi_j\ \ldots\ \psi_m]$ is a complex matrix whose columns consist of mutually orthogonal coordinate-dependent eigenvectors, i.e. $\mathbf{\Psi}_X(\omega)\mathbf{\Psi}^H_X(\omega) = \mathbf{I}$, being $\mathbf{\Psi}^H_X(\omega)$ the complex conjugate transpose of $\mathbf{\Psi}_X(\omega)$. It is stressed that for Hermitian matrices, eigenvalues and singular values are closely related: since all eigenvalues are non-negative, $\lambda_i(\omega) \geq 0$, these are also singular values whose corresponding singular vectors $\psi_i(\omega)$ coincide with the eigenvectors [34].

Once the nodal response processes $X_i(t)$ ($i = 1, .., m$) of a given structural system are known, it is possible to identify the dynamic eigenparameters characterizing the structure only via the eigenvalue decomposition of the output PSD matrix if a constant Power Spectral Density is assumed for the input, i.e. $S_F(\omega) = C$ (white noise assumption):

$$\mathbf{S}_X(\omega) = \mathbf{H}(\omega)\mathbf{S}_F(\omega)\mathbf{H}^H(\omega) = \mathbf{H}(\omega)\mathbf{C}\mathbf{H}^H(\omega) \tag{27}$$

The diagonalization of the spectral density matrix, namely the eigenvalues plotting, yields the eigenfrequencies as local maxima and allows to detect even closely spaced modes, since more than one eigenvalue can reach a local maximum around the close eigenfrequency. In detail, each eigenvalue $\lambda_i(\omega)$ denotes the vibration energy of a certain mode, whereas each eigenvector $\psi_i(\omega)$ is an estimation of the mode shape corresponding to a certain eigenvalue. Moreover, eigenvalues shifts allow to catch the presence of damage in the structure as they are frequency-dependent parameters and eigenvectors changes provide spatial information about the damage position as they are coordinate-dependent parameters.

It is worth noting that when the structure is subjected to a univariate unidimensional random vibration, as in case of seismic action, the response $X(t)$ of the system to a dynamic loading $F(t)$e equals:

$$\mathbf{X}(\omega, T) = F(\omega, T)\mathbf{H}(\omega)\mathbf{e} \tag{28}$$

where e is a constant influence vector indicating the spatial distribution of the force acting on the system while $F(\omega, T)$ represents the Fourier Transform of the univariate stochastic process. In such a case, the ratio between the response signals results independent of the input component acting in their same direction, as shown:

$$\frac{\underline{X_j}(\omega)}{X_j(\omega)} = \frac{\sum_{k=1}^n H_{ik}(\omega)e_k F(\omega, T)}{\sum_{k=1}^n H_{jk}(\omega)e_k F(\omega, T)} \Rightarrow \frac{\underline{X_j}(\omega)}{X_j(\omega)} = \frac{\sum_{k=1}^n H_{ik}(\omega)e_k}{\sum_{k=1}^n H_{jk}(\omega)e_k} \tag{29}$$

This implies the independence of the system's spectral response when univariability and unidimensionality of the excitation are assumed. As a consequence, the PSD method results suitable for output-only identification techniques as well as input–output techniques.

Regarding the derivatives of spectral density functions involving the stochastic derivative of a process, their relationships are given by the expressions below:

$$S_{\dot{X}}(\omega) = \omega^2 S_X(\omega) \qquad S_{\ddot{X}}(\omega) = \omega^4 S_X(\omega) \tag{30}$$

This means that once the matrix of spectral accelerations is known, it is always possible to go back to the matrix of spectral displacements and vice versa, since a proportional ratio of one to ω^4 between these spectral processes is established.

3.2. Spectral damage index and algorithm parameters

The spectral-based damage identification method is based on the consideration that Power Spectral Density functions explicitly depend on the frequency contents of the related nodal processes, therefore changes in the system's stiffness caused by evolutionary damage scenarios are in turn reflected by changes in its response power spectrum matrix as well as its eigenparameters.

Let us consider a multivariate stochastic vector process $X(t)$ with power spectrum matrix $S_X(\omega)$. In [35] it has been shown that $X(t)$ can be expressed as a summation of n independent fully coherent stochastic processes as follows:

$$\mathbf{X}(t) = \sum_{k=1}^{n} \mathbf{Y}_k(t) \tag{31}$$

where

$$\mathbf{Y}_k(t) = \int_{-\infty}^{+\infty} \boldsymbol{\psi}_k(\omega) \lambda_k(\omega)^{1/2} e^{i\omega t} dB_k(\omega) \tag{32}$$

in which $\boldsymbol{\psi}_k(\omega)$ and $\lambda_k(\omega)$ are the kth eigenvector and eigenvalue of $S_X(\omega)$ and $B_k(\omega)$ is a zero-mean normal complex process having orthogonal increments:

$$E[dB_k(\omega)] = 0 \qquad dB_k(\omega) = dB_k^*(-\omega) \qquad E[dB_r(\omega) dB_s^*(\omega)] = \delta_{\omega r \omega s}\, d\omega_r \tag{33}$$

where the star means complex conjugate and δ is the Kronecker delta ($\delta_{\omega r \omega s} = 1$ if $\omega_r = \omega_s$, $\delta_{\omega r \omega s} = 0$ if $\omega_r \neq \omega_s$).

In discretized version, Eq. (32) becomes:

$$\mathbf{Y}_k(t) = 2\,\mathrm{Re}\left[\sum_{j=1}^{m} \boldsymbol{\psi}_k(\omega_j) \sqrt{\lambda_k(\omega_j) \cdot \Delta\omega_j}\, P_j^{(k)} e^{i\omega_j t} \right] \tag{34}$$

where Re[•] returns the real part of the complex value expression and $P_j^{(k)}$ is a random complex number defined as follows:

$$P_j^{(k)} = R_j^{(k)} - iI_j^{(k)} \tag{35}$$

$R_j^{(k)}$ and $I_j^{(k)}$ being zero-mean normal random numbers obeying the following orthogonality relationships:

$$E\left[R_j^{(r)} R_j^{(s)}\right] = \frac{1}{2}\delta_{jk}\delta_{rs} \qquad E\left[I_j^{(r)} I_j^{(s)}\right] = \frac{1}{2}\delta_{jk}\delta_{rs} \qquad E\left[R_j^{(r)} I_j^{(s)}\right] = 0 \tag{36}$$

and δ is the Kronecker delta ($\delta_{jk} = 1$ if $j = k$, $\delta_{jk} = 0$ if $j \neq k$).

Let us assume that $X^d(t)$ is a damaged multivariate stochastic vector process, then Eq. (31) and Eq. (32) can be rewritten in the form:

$$\mathbf{X}^d(t) = \sum_{k=1}^{n} \mathbf{Y}_k^d(t) \tag{37}$$

$$\mathbf{Y}_k^d(t) = \int_{-\infty}^{+\infty} \boldsymbol{\psi}_k^d(\omega) \lambda_k^d(\omega)^{1/2} e^{i\omega t} dB_k(\omega) \tag{38}$$

and the difference between the two vector processes can be expressed as shown below:

$$\Delta\mathbf{X}(t) = \mathbf{X}^d(t) - \mathbf{X}(t) = \sum_{k=1}^{m} \left(\mathbf{Y}_k^d(t) - \mathbf{Y}_k(t) \right) \tag{39}$$

Replacing Eq. (32) and Eq. (38) in Eq. (39), one obtains:

$$\Delta\mathbf{X}(t) = \sum_{k=1}^{m} \int_{-\infty}^{+\infty} \Delta\boldsymbol{\psi}_k(\omega) \cdot e^{i\omega t} dB_k(\omega) \tag{40}$$

where

$$\Delta\boldsymbol{\psi}_k(\omega) = \boldsymbol{\psi}^d_k(\omega)\lambda^d_k(\omega)^{1/2} - \boldsymbol{\psi}_k(\omega)\lambda_k(\omega)^{1/2} \tag{41}$$

Similarly, in discretized version, Eq. (40) turns into:

$$\Delta\mathbf{X}(t) = 2\Delta\omega\,\mathrm{Re}\left\{\sum_{k=1}^{m}\sum_{j=1}^{n}\Delta\boldsymbol{\psi}_k(\omega_j)\cdot P^{(k)}e^{i\omega_j t}\right\} \tag{42}$$

where

$$\Delta\boldsymbol{\psi}_k(\omega_j) = \boldsymbol{\psi}^d_k(\omega_j)\sqrt{\lambda^d_k(\omega_j)} - \boldsymbol{\psi}_k(\omega_j)\sqrt{\lambda_k(\omega_j)} \tag{43}$$

The equations above show that the difference between reference and damage multivariate stochastic vector processes depends on both eigenvectors and eigenvalues estimated from the PSD matrix of the two processes. It is worth noting that the complex function $\Delta\boldsymbol{\psi}_k(\omega_j)$ plays the role of a natural damage indicator since when $\Delta\boldsymbol{\psi}_k(\omega_j) = 0$ for any k and j then $\Delta\mathbf{X}(t) = \mathbf{X}^d(t) - \mathbf{X}(t) = 0$, meaning that no damage occurs in the structure, i.e. $\mathbf{X}^d(t) = \mathbf{X}(t)$.

Taking this into account, the following spectral index has been defined for identifying the structural damage:

$$\Delta\boldsymbol{\psi} = \sum_{k=1}^{m}\left|\left|\sum_{j=1}^{n}\left[\boldsymbol{\psi}^d(\omega_j)\sqrt{\lambda^d_k(\omega_j)}\right]\right| - \left|\sum_{j=1}^{n}\left[\boldsymbol{\psi}^u(\omega_j)\sqrt{\lambda^u_k(\omega_j)}\right]\right|\right| \tag{44}$$

Basically, the index $\Delta\boldsymbol{\psi}$ is a damage indicator given by the difference between spectral modes estimated through the amplification of the eigenvectors extracted from the response PSD matrix by the square root of the corresponding eigenvalues. If no damage occurs in the structure, then $\Delta\boldsymbol{\psi}_k(\omega_j) = 0$ for any k and j since $\boldsymbol{\psi}^d_k(\omega_j)\sqrt{\lambda^d_k(\omega_j)} = \boldsymbol{\psi}^u_k(\omega_j)\sqrt{\lambda^u_k(\omega_j)}$ and $\left|\sum_{j=1}^{n}\boldsymbol{\psi}^d_k(\omega_j)\sqrt{\lambda^d_k(\omega_j)}\right| = \left|\sum_{j=1}^{n}\boldsymbol{\psi}^u_k(\omega_j)\sqrt{\lambda^u_k(\omega_j)}\right|$, thus the index $\Delta\boldsymbol{\psi}$ in Eq. (44) equals zero. When a damage occurs in the structure, summing up over the whole frequency domain, the absolute value of the difference $|\Delta\boldsymbol{\psi}_k| = \left|\left|\sum_{j=1}^{n}\boldsymbol{\psi}^d_k(\omega_j)\sqrt{\lambda^d_k(\omega_j)}\right| - \left|\sum_{j=1}^{n}\boldsymbol{\psi}^u_k(\omega_j)\sqrt{\lambda^u_k(\omega_j)}\right|\right|$ for a given k is different than zero and is related to the magnitude of the damage. The index $\Delta\boldsymbol{\psi}$ considers the summation of each $|\Delta\boldsymbol{\psi}_k|$, viz. $\Delta\boldsymbol{\psi} = \sum_{k=1}^{m}|\Delta\boldsymbol{\psi}_k|$, taking into account the contribution of all the estimated spectral modes, each one appropriately weighed over the whole frequency domain by means of the respective non-zero eigenvalue. Although the modes effectively dominating the structural response of a system are usually reduced to a limited number, this approach will lead to a more complete damage investigation procedure. However, if possible damage locations are known in advance, the PSD algorithm can be computed just taking into account the eigenvectors related to those target points. Note that, dealing with complex modes, the introduction of absolute values in Eq. (44)

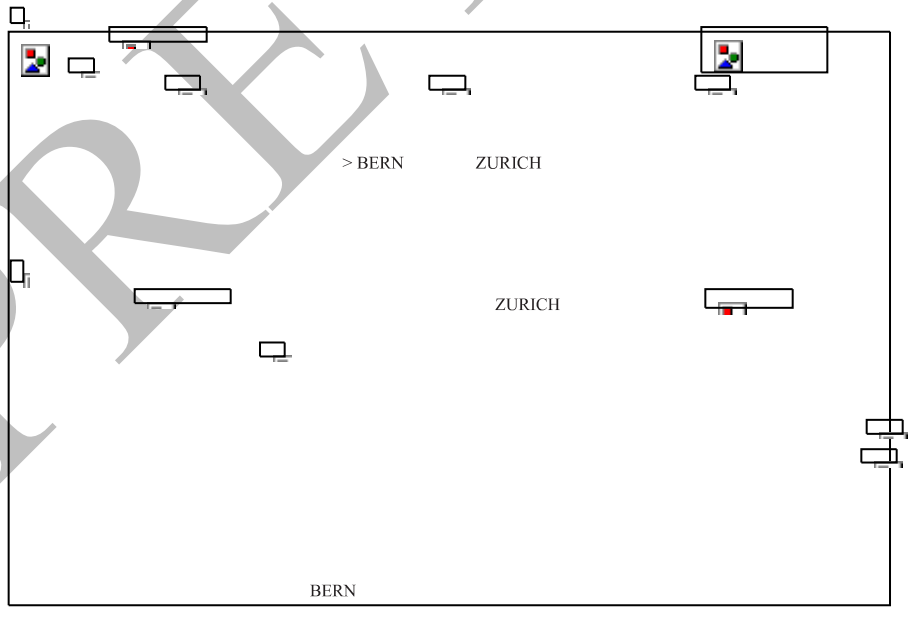

Fig. 1. Z24 Bridge: longitudinal section (a) and top view (b) (adapted from [41]).

is mandatory: it is mathematically proved that the difference between absolute values of complex numbers does not coincide with the absolute value of their difference.

The so-defined spectral damage localization index will result in a vector of scalars whose magnitude enables to identify the damage position in the system and to give a qualitative estimate of the damage size. Each scalar is associated with the damage of a certain DOF and the dimension of the vector is given by the total number of measured DOFs. To facilitate the interpretability of the results, the index can be expressed in the range [0–1] by dividing each of its components by the component with the maximum value, i.e. $\Delta\hat{\psi} = \Delta\psi/\max|\psi_i|$. If only one Damage Scenario (DS) is available besides the Reference Scenario (RS), the parameters used in the algorithm computation will regard the damaged and undamaged conditions, whereas if data from several DSs are collected, a relative index can be computed and the evolution of the damage can be progressively followed up to the last scenario. It is stressed that the interpretation of the index is univocal and independent of the type of signals used for its estimation.

In short, the PSD approach for damage identification consists of the following basic steps:

(1) Construction of the response power spectrum matrix;
(2) Eigenparameters decomposition of the matrix;
(3) Spectral damage index computation.

4. Application of the PSD method to the Z24 Bridge

The numerical simulation hereafter described will better illustrate the approach presented in the previous section. As mentioned in Section 1, the case study chosen to analyze and validate the spectral-based method is the Z24 Bridge. For this purpose, several linear transient analyses are performed to collect the dynamic response of the system to different types of excitation and with respect to two structural conditions, namely undamaged and damaged.

4.1. Description of the bridge

Located in Switzerland and dated back to the 1960s, this bridge was an overpass of the national highway A1 (Bern/Zurich) linking the villages of Koppigen and Utzenstorf. The main geometrical features of the concrete bridge were: a mid-span of 30 m, two side spans of 14 m each and two cantilevers of 2.7 m, for a total length of 63.4 m (Fig. 1a). The cross-section of the bridge girder was 8.6 m wide and consisted of two box cells with 16 post-tensioned cables in the three webs (Fig. 2). The two intermediate piers supporting the structure were clamped into the girder, while the triplets of columns at both ends were connected to the girder via hinges. All the supports were rotated with respect to the longitudinal axis of the structure yielding a skew bridge (Fig. 1b). Columns and abutments were completely embedded in the soil. After being monitored for one year, the bridge was artificially damaged in order to study its dynamic response when subjected to progressive damage scenarios, corresponding to realistic and relevant cases. Ambient vibration tests were performed to collect the data before and after applying each DS, using the vibrations due to the traffic beneath the bridge as operational conditions. Details about the experimental data can be found in [36]. A full description about the sequence and extent of the different damage scenarios is given in [37] and [40]. The damage scenario considered in this paper is the settlement of the pier foundation, simulated by lowering the right supporting pier (at 44 m) by 95 mm and inducing cracks in the bridge girder right above (Fig. 3).

4.2. FE model calibration

A simplified FE model was built in DIANA [38] software and calibrated using the dynamic features extracted from the experimental data. The model consists of 126 beam elements for girder, piers and abutment columns. In addition, 6 point mass elements with concentrated translational mass and rotary inertia components are considered for cross girders and foundations. The soil under piers foundation and abutments is simulated by 22 spring elements (Fig. 4). The initial values of the soil stiffness are: $K_{v,p}$ ¼ 180 10^6 N/m, $K_{h,p}$¼ 210 10^6 N/m (under the piers, at 14 and 44 m), $K_{v,c}$¼ $K_{h,c}$¼ 100 10^6 N/m (under the columns, at zero and 58 m); $K_{v,a}$¼180 10^6 N/m, $K_{h,a}$¼200 10^6 N/m (at the abutments) and $K_{v,ac}$ ¼ $K_{h,ac}$¼ 100 f0 N/m (around the columns). The concrete is considered to be homogeneous with initial values of E_0 ¼37.5 GPa for Young's modulus and V¼0.2 for Poisson's ratio. Note that the girder has higher stiffness on top of the supporting piers because of an increased thickness of bottom and top girder slabs. The cross-section area, moments of inertia and torsional moments of inertia are pre-calculated and given as input. Being the geometrical features of the bridge known,

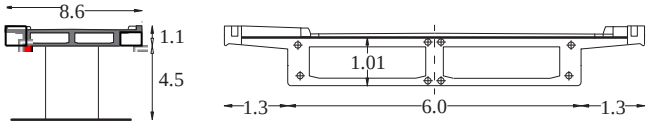

Fig. 2. Cross-section of the bridge [41].

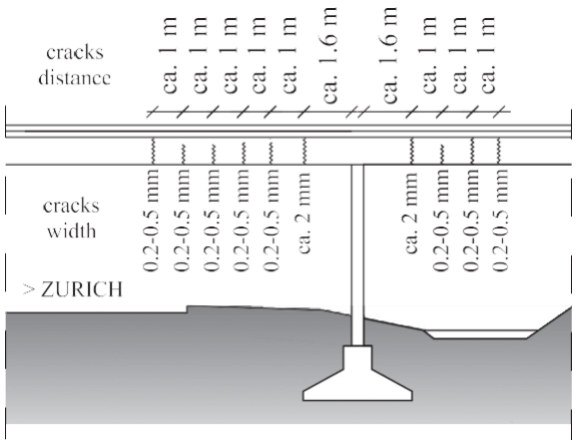

Fig. 3. Cracks in the bridge girder after lowering the pier at 44 m (adapted from [36]).

Fig. 4. Z24 FE beam model: springs elements (gray boxes) and point mass elements (black dots). The excitation points (1, 2 and 3) for impulse, ramp and shaking forces are also indicated.

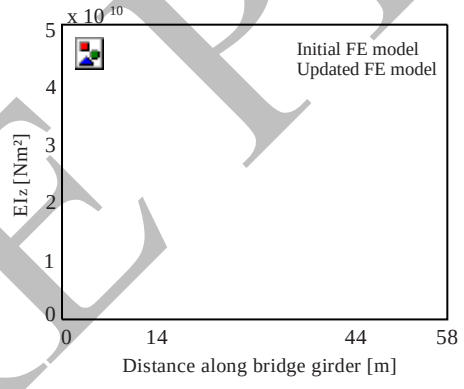

Fig. 5. Initial and updated bending stiffness distribution along the girder of the FE model simulating the Z24 Bridge.

Table 1
Experimental, initial and updated eigenfrequencies for the reference scenario.

Mode	Eigenfrequencies [Hz] Experimental	FE model		Error [%]
		Initial value	Updated value	
1	3.89	3.88	3.89	þ0.1
2	5.02	5.27	4.93	−1.9
3	9.80	8.56	9.17	−6.4
4	10.30	10.60	10.56	þ2.5
5	12.67	13.80	13.28	þ4.8
|Average|	–	–	–	3.1

the bending stiffness distribution along the girder is computed only updating the values of Young's modulus, so as to minimize the difference between experimental and analytical modal parameters. The first five identified eigenfrequencies are used for the responses correlation. Fig. 5 displays the initial and updated bending stiffness distribution along the bridge girder. The updated eigenfrequencies are shown in Table 1. Regarding the numerical mode shapes, the first and fourth are bending modes, symmetric and non-symmetric respectively (Fig. 6), the third and fifth are transversal modes and the second is a longitudinal mode. Since the damage scenario that will be referred to basically affects the bending behavior of the bridge, the vertical modes only are considered in this study. The experimental results are well approximated, because five frequencies can be accurately reproduced. Still, it would have been desirable to validate the mode shapes information and to use them in the model updating process. However, this information was not available.

4.3. *Preliminary eigenvalue analysis*

Before proceeding to the spectral-based damage identification, a preliminary eigenvalue analysis of the bridge in its reference configuration is carried out to select the measurements points, the sampling frequency and the total sampling time for the data tabulation. Further eigenvalue analyses are then performed to evaluate the response of the system for three different damage scenarios (DS_I, DS_{II} and DS_{III}), numerically simulated with the objective of replicating the damage introduced in the real structure by the settlement of the Koppigen support. Indicated by the Roman numeral as subscript, the damage scenarios consist of progressive Young's modulus reductions of the girder above the Koppigen pier. As the pier lowers the structure cracks and this reduces the stiffness, thus the pier lowering of 95 mm is implicitly considered in Young's modulus reduction. Particularly, DS_I consists of a 30% reduction of Young's modulus in the beam elements of the girder progressively approaching to the settled pier; DS_{II} consists of a 60% reduction of the Young's modulus in the beam elements of the girder just above the Koppigen pier and DS_{III} is a combination of DS_I and DS_{II}. A comparison between measured and numerical frequencies has been used to help the selection of the damage scenario better simulating the settlement of the pier foundation induced in the real structure. Table 2 presents the eigenfrequencies comparison among the three damage scenarios. Even if the average error is not so different in the considered scenarios, it is noted that only DS_{II} and DS_{III} approximate well the first frequency. From these two, DS_{II} is the one with the smallest error and is, thus, chosen as representative of the damaged configuration. The location of the assumed damage scenario is schematized in Fig. 7.

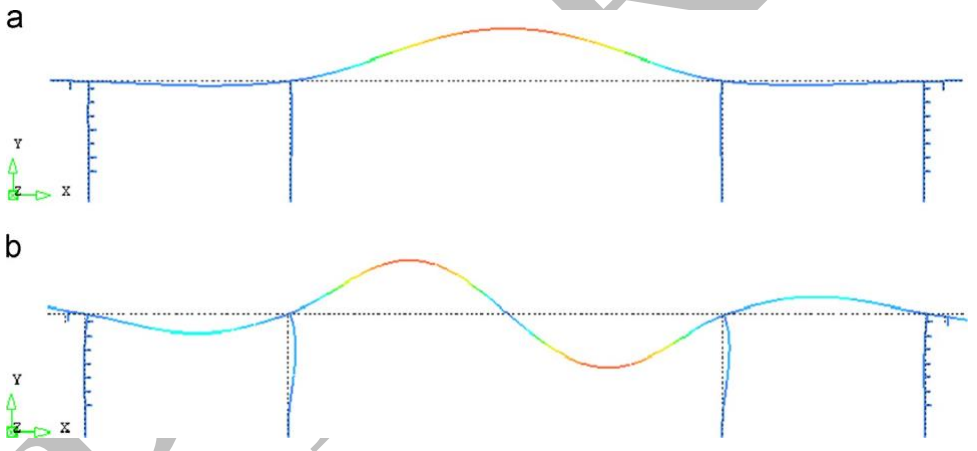

Fig. 6. Bending mode shapes from the eigenvalue analysis: first (a) and fourth (b) mode.

Table 2
Experimental and numerical eigenfrequencies for different damage scenarios (EMA indicates Experimental Modal Analysis and Δ_ω is the average of the absolute value of the errors).

Mode	Eigenfrequencies [Hz]					
	Undamaged		Damaged			
	EMA	FE model	EMA	FE model		
				DS_I	DS_{II}	DS_{III}
1	3.89	3.89	3.67	3.77	3.69	3.67
2	5.02	4.93	4.95	4.86	4.82	4.80
3	9.80	9.17	9.21	8.54	8.57	8.36
4	10.30	10.56	9.69	10.24	10.33	10.31
5	12.67	13.28	12.03	13.11	13.04	13.01
Δ_ω [%]	–	3.13	–	5.29	5.02	5.36

4.4. Linear dynamic analysis for reference and damage scenarios

After defining the two structural conditions representative of the structure in the reference and damage configurations, and in order to compute the spectral damage index, four types of excitation are numerically generated and applied to both configurations with the aim of collecting the nodal response processes of 23 measurement points (Fig. 7) and build the PSD matrix. The types of excitation source applied to the bridge deck are:

(1) Triangular pulse: a force of 1000 kN is hitting the deck for a very short time;
(2) Ramp force: a force reaching the maximum value of 2000 kN is suddenly released to allow free vibration;
(3) Random vibrations: point-to-point different Gaussian white noise signals are generated to simulate ambient vibration (traffic, wind, micro-earthquakes) acting along the bridge;
(4) Shaker: a band-limited input signal is exciting the bridge deck in the frequency range 3–15 Hz.

Except for the case of random vibrations, all the other inputs are exciting the structure in three different points: (1) at one quarter of the main span, (2) in the middle of the Utzenstorf side-span and (3) at one third of the Koppigen side-span (see Fig. 4). All the data are sampled at 100 Hz, but the measurement time differs depending on the type of input, reading 80 s for triangular impulse and ramp force, 300 s for the shaker and 10 min for random vibrations. This results in 7999 data

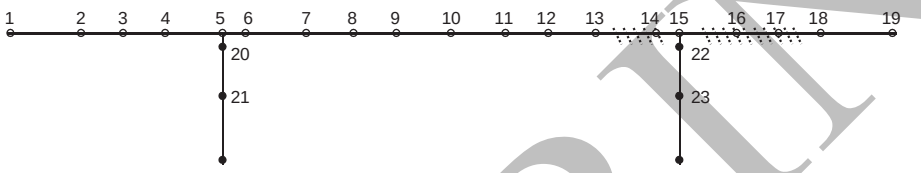

Fig. 7. Schematization of the assumed damage scenario DS_{II} (dot lines) and indication of the measurement points considered along the bridge for generating an artificial dynamic response.

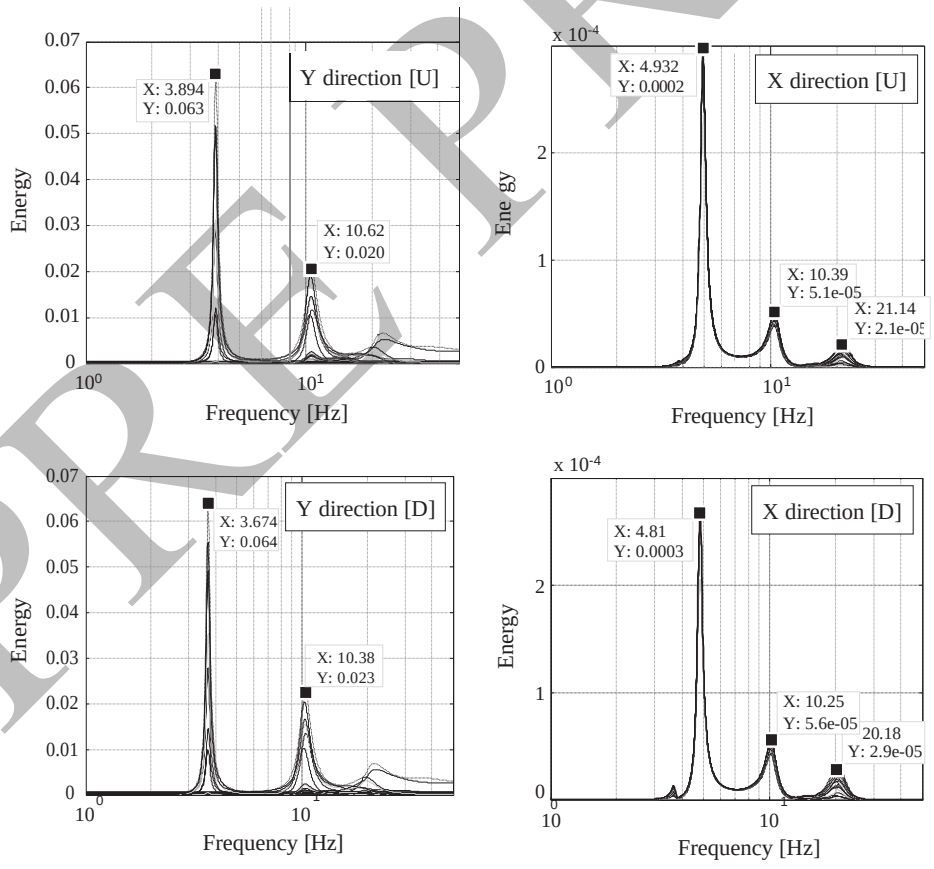

Fig. 8. Eigenvalues plotting for impulse excitation (U and D stand for undamaged and damaged conditions). The number of singular values plotted equals the number of measurement points.

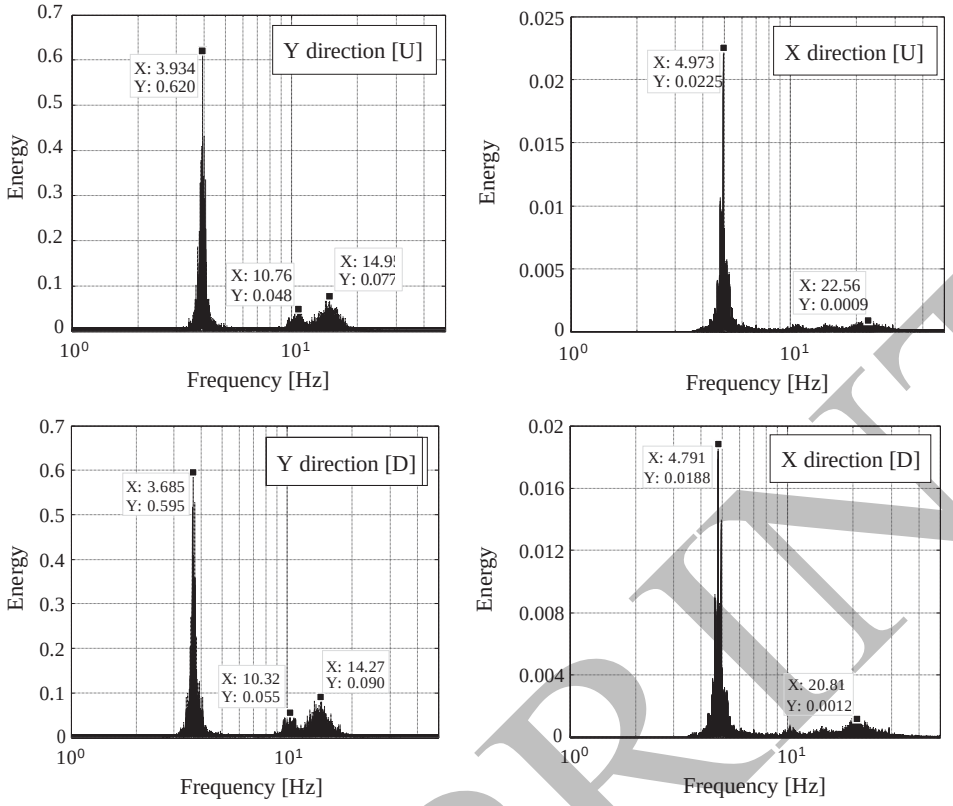

Fig. 9. Eigenvalues plotting for random vibrations (U and D stand for undamaged and damaged conditions). The number of singular values plotted equals the number of measurement points.

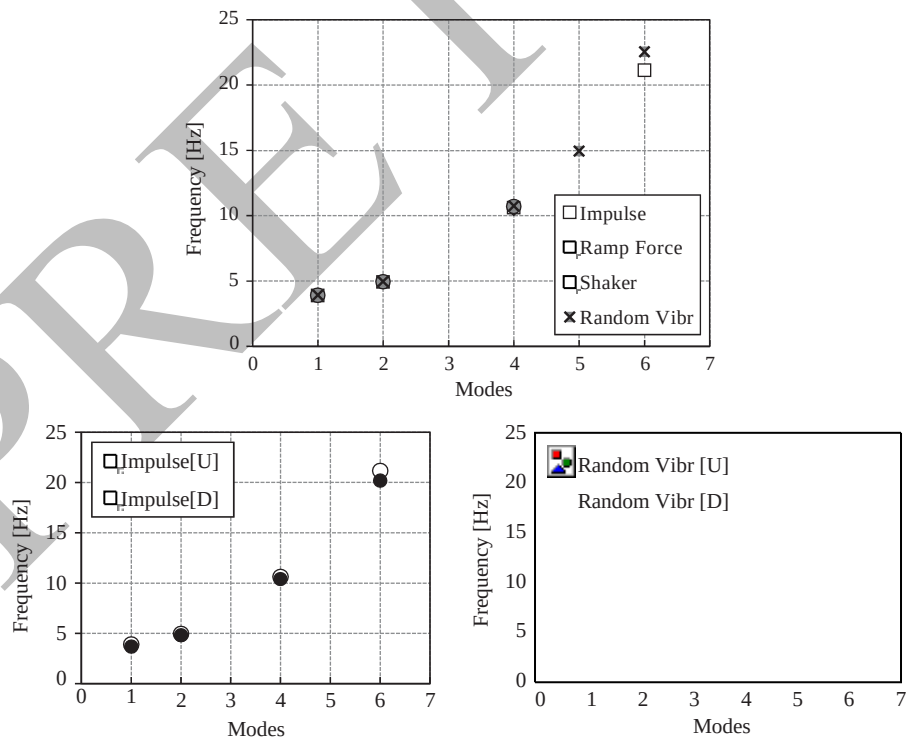

Fig. 10. Eigenfrequencies comparison for different excitation sources.

points per channel for the first two excitations, 29999 points per channel for the third excitation and 59999 points per channel for the last excitation.

Dealing with force vectors varying in time, a time-stepping procedure is needed to compute the structural response, thus a series of linear transient analyses are carried out in DIANA making use of Newmark's method. Both the time variation of the excitation (Δt¼ 0.01 s) and the shortest natural period of interest of the structure (T_n¼0.045 s) are taken into account to choose the best time step Δt for the analysis (preferably, Δt¼ T_n/20), resulting in a Δt¼ 0.002 s. Nevertheless, to ensure the stability of the method for any Δt, values of γ¼ 1/2 and β¼ 1/4 are adopted for the integration parameters, based on the assumption of the constant average acceleration method. A damping ratio of 1% [10] is considered in the computation of the Rayleigh damping coefficients to set for the dynamic analysis and a linear behavior of the structure is assumed, meaning that no equilibrium iterations are required.

4.5. *Spectral-based damage identification of the bridge*

After collecting all the acceleration time-histories from the different analyses, the second order properties of the nodal processes are computed and the spectrum-driven method is applied to each case. The PSD estimates are obtained via MATLAB (2010) from the N-point DFTs of the relevant nodal response processes sampled at 100 Hz, where N is the next power of two greater than the length of the signal. In detail, for the impulse and ramp force cases, the power spectrum is split into 4096 bins, resulting in a frequency resolution (FR) of 0.012 Hz/bin; for the shaker case, the spectrum is divided into 16384 bins, thus the FR equals 0.003 Hz/bin; finally, for the random case, the power spectrum is split into 32768 bins, reading a FR of 0.0015 Hz/bin. Moreover, the default Hamming window with 50% overlap is applied to estimate the cross PSDs, except for the case of random data in which a Hanning window with 50% overlap is used. It needs to be highlighted that the damage scenario selected for the comparison with the reference scenario mostly affects the bending behavior of the bridge deck and supporting piers. As a consequence of that, the transversal direction (z) has not been considered in the subsequent damage analysis, also because of the low amplitude of the acceleration responses in that direction. Therefore, two [23x23] square spectral matrices have been built: one from the output signals in horizontal direction (x) and the other one from the output signals in vertical direction (y).

The next step of the procedure consists of the solution of the eigenvalue problem formulated in Section 3.1 and the subsequent diagonalization of the matrix in order to estimate the eigenfrequencies. Figs. 8 and 9 show the eigenvalues plotting for both structural conditions in the two directions investigated, with regards to impulse and random excitations, as selected examples of different types of excitation. The results for the four excitations are compared in Fig. 10, Tables 3 and 4. As it can be seen, for shaker and ramp force three modes of vibration are identified, whereas for impulse and random vibrations four and five modes are estimated, respectively. The frequency change between sound and damaged conditions comes from the stiffness degradation of the bridge girder, numerically simulated by reducing Young's

Table 3
Comparison of identified eigenfrequencies among the four excitation types.

Mode	Eigenfrequencies [Hz]							
	Undamaged				Damaged			
	Impulse	Ramp	Shaker	Ambient	Impulse	Ramp	Shaker	Ambient
1	3.89	3.89	3.91	3.93	3.67	3.67	3.68	3.69
2	4.93	4.93	4.95	4.97	4.81	4.81	4.82	4.79
3	–	–	–	–	–	–	–	–
4	10.62	10.49	10.70	10.76	10.38	10.23	10.35	10.32
5	–	–	–	14.95	–	–	–	14.27
6	21.14	–	–	22.56	20.18	–	–	20.81

Table 4
Frequencies changes between undamaged and damaged configurations for all the four excitations (Δ_ω^* is the average of the frequency difference of the first three identified modes and Δ_ω is the average of the frequency difference of all the estimated modes).

Mode	Frequency difference [%]			
	Impulse	Ramp force	Shaker	Ambient
1	– 5.66	– 5.66	– 5.88	– 6.11
2	– 2.43	– 2.43	– 2.63	– 3.62
3	–	–	–	–
4	– 2.26	– 2.48	– 3.27	– 4.09
5	–	–	–	– 4.55
6	– 4.45	–	–	– 7.76
Δ_ω [%]*	– 3.45	– 3.52	– 3.93	– 4.61
Δ_ω [%]	– 3.70	– 3.52	– 3.93	– 5.22

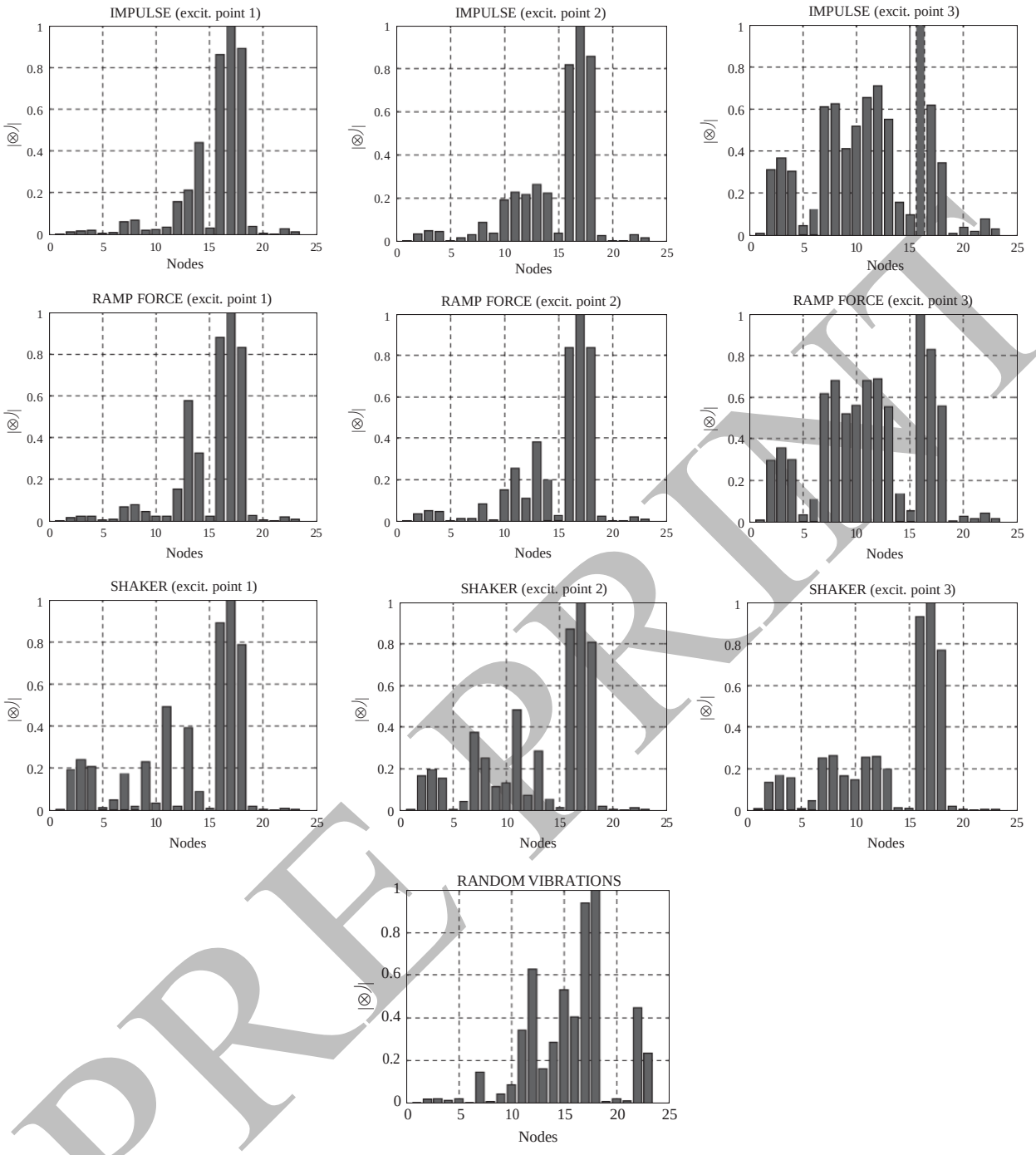

Fig. 11. Damage localization by PSD method: comparison of the results with respect to the type and location of the excitation sources.

modulus. In particular, an overall decrease up to 3.93% and 4.61% can be noticed during the simulation of shaker and random vibrations tests. This allows to qualitatively detect the presence of damage in the bridge, but that does not provide any spatial information about it.

5. Discussion of the results

To localize the damage, the PSD algorithm described in Section 3.2 has been adopted for all the different excitation sources. Unlike the eigenvalues plotting, only the spectral output signals in vertical direction have been used for the index

computation, as the damage scenario selected prevalently influences bending modes. The results obtained are displayed in Fig. 11. The number of bars coincide with the measurement points (Fig. 7), viz. with the damage position, whereas the size of each bar $\Delta\psi$ (or the difference between spectral modes) gives a qualitative estimate of the damage size affecting that particular node or the area close by.

The application of the PSD method to the Z24 Bridge using data sets from different excitation sources has allowed to weigh the sensitivity of the damage index with respect to the type and spatial distribution of the input signals.

In the first analysis, the bridge deck is excited by a symmetrical triangular pulse with an extremely short duration t_d, when compared to the natural period T_n of the system, so it can be referred to the limit case of pure impulse with t_d/T_n approaching to zero and flat spectrum. In particular, for the case of impulse applied at one quarter of the middle span (excitation point 1), the plotting of the spectral index pinpoints the damage exactly in the nodes corresponding to the area in which Young's modulus has been reduced, but with higher peaks towards the Koppigen (right) side. As expected, no damage affects node 15 since the girder above the settled pier starts cracking at a certain distance from the joint and Young's modulus has been reduced on the base of this damage scenario. Identical peaks can be noticed changing the excitation point from the middle span to the Utzenstorf side-span, whereas false positives are detected exciting the structure close to the damage area, on the Koppigen side-span.

In the second analysis, a linear increasing force with finite rise time and flat spectrum excites the bridge. For all the three excitation points, the algorithm plotting gives peaks consistent with the ones obtained from impulse data. Still, false positives are identified when the system is excited in the vicinity of the damaged region. It is highlighted that, even though the spectral damage localization index may yield false positives, indicating that damage is present when none exists, it does not yield false negatives which would indicate the absence of dangerous situations when damage exists.

Regarding the random vibrations data, it needs to be stressed that the numerical nature of the excitations made the output signals pretty noisy and difficult to analyze. Due to that, the eigenfrequencies identification from the eigenvalue plotting is a very hard task and the presence of unclear peaks affects the results of the damage localization, since the eigenvalues are the weighing factors of the spectral index and each eigenvector is related to its own eigenvalue. Therefore, moderate results have been obtained from the index computation, e.g. inconsistent peaks are detected in nodes 11 and 12. When more local maxima (eigenfrequencies) are yielded by the eigenvalues, the changes in the spectral modes caused by the damage begin to occur less locally and the damage indicator spreads around the damage location, leading to false positives in the neighboring regions, e.g. in the girder to pier connection (node 15) and in the Koppigen pier (nodes 22 and 23).

Finally, to test the efficiency and variability of the spectrum-driven method when applied to data obtained from input–output identification techniques for which the input is not characterized by a flat spectrum, a shaker test simulation is carried out. This input has been generated to replicate the harmonic force due to counter rotating masses exciting the bridge with an amplitude proportional to the excitation frequency. It is known that this type of excitation makes the identification of low frequency modes difficult, and it is also impractical to obtain the static response of the structure [37]. Nevertheless, even if the input is characterized by a spectrum not completely flat, the eigenvalues are amplified right at the resonant frequencies and the PSD algorithm seems not to be affected by the memory of the input in the spectral responses. In fact, the index plotting

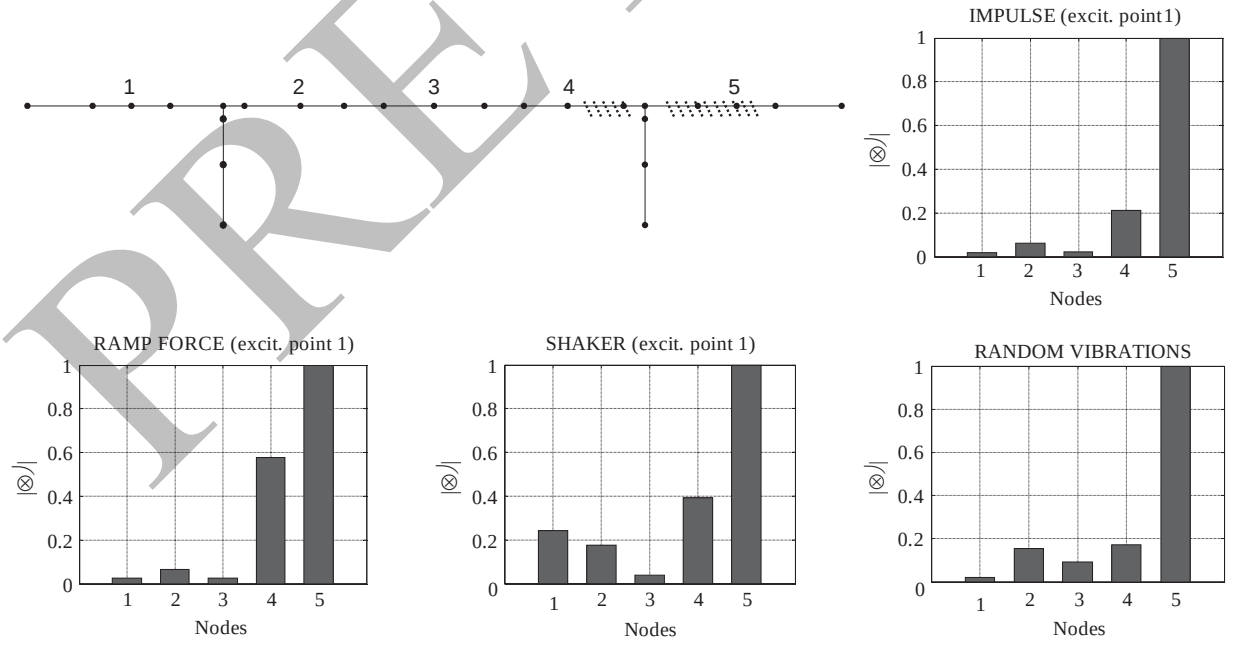

Fig. 12. Results of the spectral damage localization index after reducing the number of measured DOFs.

Table 5
List of selected damage identification methods.

Method	Level	Modal parameters	Damage index	Criterion for damage identification
COMAC	2	Mode shapes φ or modal curvatures φ″	$\frac{\left\lvert\sum_{j=1}^{m} \varphi_{i,j}^{u} \varphi_{i,j}^{d}\right\rvert^2}{\sum_{j=1}^{m} (\varphi_{i,j}^{u})^2 \sum_{j=1}^{m} (\varphi_{i,j}^{d})^2}$	Low values in the range [0–1]
PM	2	Mode shapes φ or modal curvatures φ″	$\sum_{j=1}^{m} [\varphi_j^d (\frac{\omega_j^u}{\omega_j^d}) - \varphi_j^u]$	High values (no threshold)
MSCM	2	Modal curvatures φ″	$\sum_{j=1}^{m} \lvert \varphi''_{d,j} - \varphi''_{u,j} \rvert$	High values (no threshold)
SCE	2	Modal curvatures φ″	$\sum_{j=1}^{m} \left\lvert \frac{\varphi''_{d,j} - \varphi''_{u,j}}{\varphi''_{u,j}} \right\rvert$	High values (no threshold)
DIM	2	Modal curvatures φ″	$\beta_{i,j} = \frac{[\int_a^b (\varphi_j^{d''})^2 dx + \int_0^L (\varphi_j^{d''})^2 dx] \int_0^L (\varphi_j^{u''}) dx}{[\int_a^b (\varphi_j^{u''})^2 dx + \int_0^L (\varphi_j^{u''})^2 dx] \int_0^L (\varphi_j^{d''}) dx}$	Normalized index values greater than 2
CFM	2–3	Mass-scaled mode shapes ϕ or modal curvatures ϕ″	$\beta = diag\{\mathbf{F}^d - \mathbf{F}^u\}; \mathbf{F} = \sum_{j=1}^{m} \frac{1}{\omega_j^2} \phi_j \phi_j^T$	High values (no threshold)

displays peaks consistent with the ones obtained analyzing data sets from other excitation sources (see Fig. 11). Additionally, no differences can be found in terms of damage localization when changing the point of application of the shaking force.

In order to evaluate the robustness of the technique, the spectral damage analysis has been repeated for all four excitation sources varying the number of measured DOFs, whereas the excitation point is maintained at one quarter of the main span. The dynamic response of the simulated bridge is now acquired in 5 points reasonably deployed along the girder, see Fig. 12. Accordingly, [5x5] power spectrum matrices have been built and decomposed for each case, resulting in a number of five eigenvalues and five eigenvectors per matrix. After estimating the spectral eigenparameters for both reference and damage configuration, the spectral damage localization index has been computed according to Eq. (44). The outcome for the four cases is shown in Fig. 12. As it can be observed, the results for simulated impulse, ramp force and shaker excitation are fairly consistent, with the damage being concentrated in the nodes 4–5, whereas for simulated random vibrations the damage is clearly pinpointed at position 5 and no false positives around the damage region are detected. It is noted that the different number of measured DOFs has not affected the outcome of the spectral damage analysis, thus the proposed method can be considered independent of the number of sensors used to acquire the system's response.

6. Comparison with other damage indexes

Aimed at assessing the performance and the strengths of the method, the proposed approach is compared with a group of VBDIMs, as disclosed in Section 2. The methods chosen for the present work mostly address the global presence of damage in the structure and they are the following: Co-ordinate Modal Assurance Criterion (COMAC); Parameter Method (PM); Mode Shape Curvature Method (MSCM); Sum of all Curvature Errors method (SCE); Damage Index Method (DIM); Changes in Flexibility Matrix method (CFM). For convenience, the damage indexes used by each method are repeated in Table 5, together with the relevant criteria to determine the presence of damage and the level of identification attempted. As highlighted in the table, the modal parameters required to compute the different indexes are either mode shapes or modal curvatures, with the exception of the CFM that requires mass-scaled parameters. Mode shapes are extracted from the simulated data by means of the Stochastic Subspace Identification (SSI) [39] method and modal curvatures are calculated from the mode shapes by the central difference theorem, or the second order approximation, as:

$$\varphi'' \approx \frac{\varphi_{i+1} - 2\varphi_i + \varphi_{i-1}}{(\Delta L^2)} \tag{45}$$

where ΔL is the distance between the measurement points i and $i+1$. Since it is assumed that the random data are acquired via OMA, mass normalized mode shapes need to be computed. The scaling factor applied to each mode and the relationship between scaled and un-scaled mode shapes can be expressed as follows:

$$\alpha = \frac{1}{\sqrt{\varphi^T \cdot \mathbf{M} \cdot \varphi}} \qquad \phi = \alpha \cdot \varphi \tag{46}$$

Note that the construction of the mass matrix used to compute the scaling factors is obtained based on the assumption of lumped masses.

All the indexes are calculated taking into account only the nodal response processes in the vertical direction, adopting the same criterion used to compute the spectral damage index. Regarding the input–output dynamic identification techniques, only the data acquired exciting the bridge at the middle span are used, since this excitation point resulted to be far enough from the

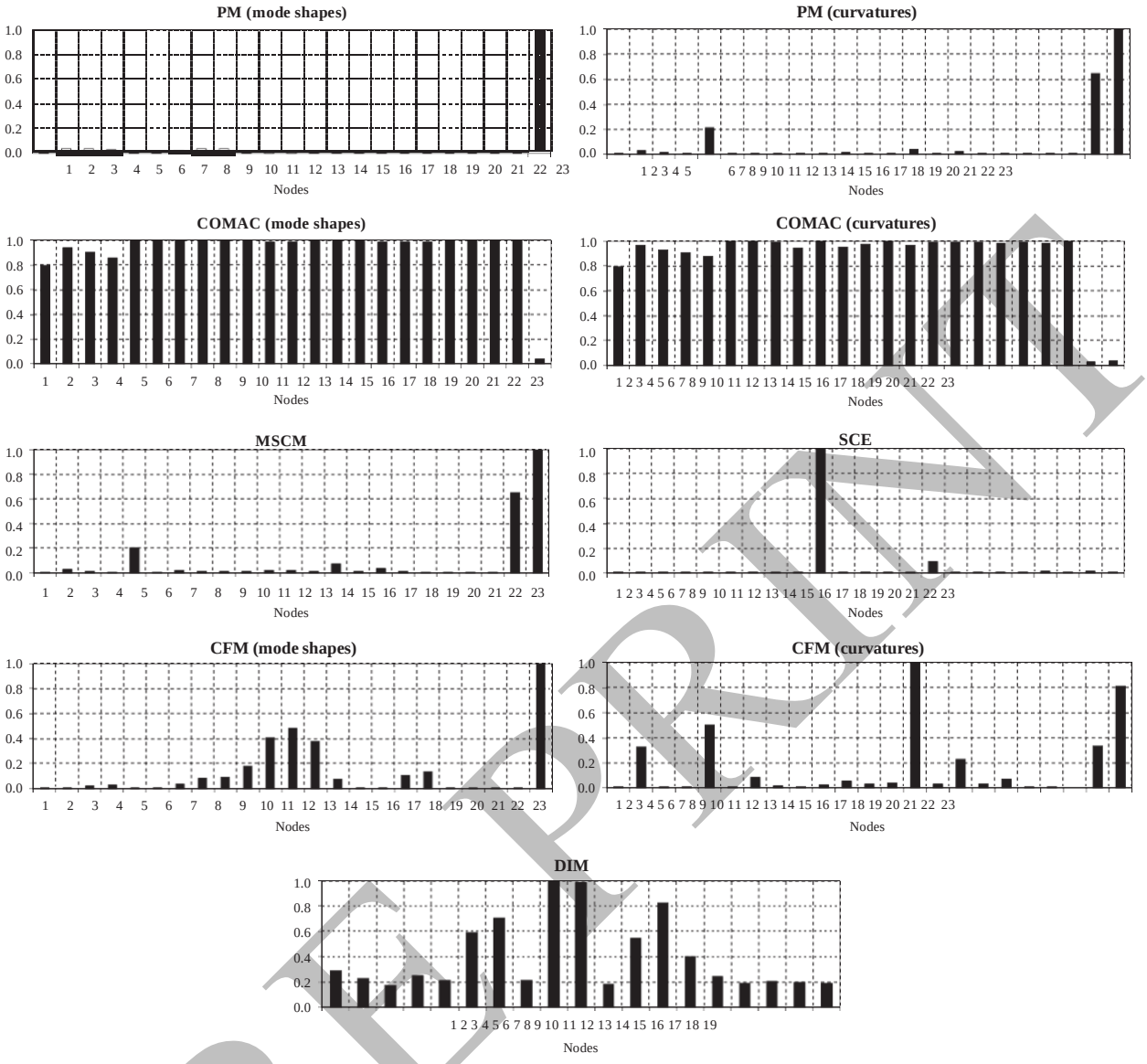

Fig. 13. Damage localization with mode shapes and modal curvatures extracted from ramp force data.

damage area in order to avoid unreliable results. The indexes extracted from the different methods are shown in Figs. 13–16. As it can be noticed, the results from the technique are strictly dependent on the type of excitation. In fact same indexes provide different results for different excitation sources even if the point of application of the input is kept the same. In particular, with regards to the ramp force case (Fig. 13), the results for COMAC, PM, MSCM and CFM are consistent since they indicate the presence of damage at the lowered pier, whereas inconsistent and unreliable results are extracted from all the indexes as far as impulse and ambient data are concerned (Fig. 14 and Fig. 16, respectively). Instead, in case of shaker simulation (Fig. 15), PM, COMAC and MSCM succeed in locating the damage, showing peaks where Young's modulus is effectively reduced, namely in the girder above the lowered pier. However, analyzing and comparing all the results it is possible to underline that, unlike the spectral index, the damage indexes selected from the literature have shown a tendency to yield ill-conditioned and not consistent results when dealing with a reduced number of measurement points and noisy signals as in the present case. This clearly demonstrates the potential of the proposed PSD method.

7. Conclusions

Based on the knowledge of the second order moments of the nodal response processes, a spectrum-driven method for damage detection and localization is proposed in this paper. In order to validate its efficiency and accuracy, the technique

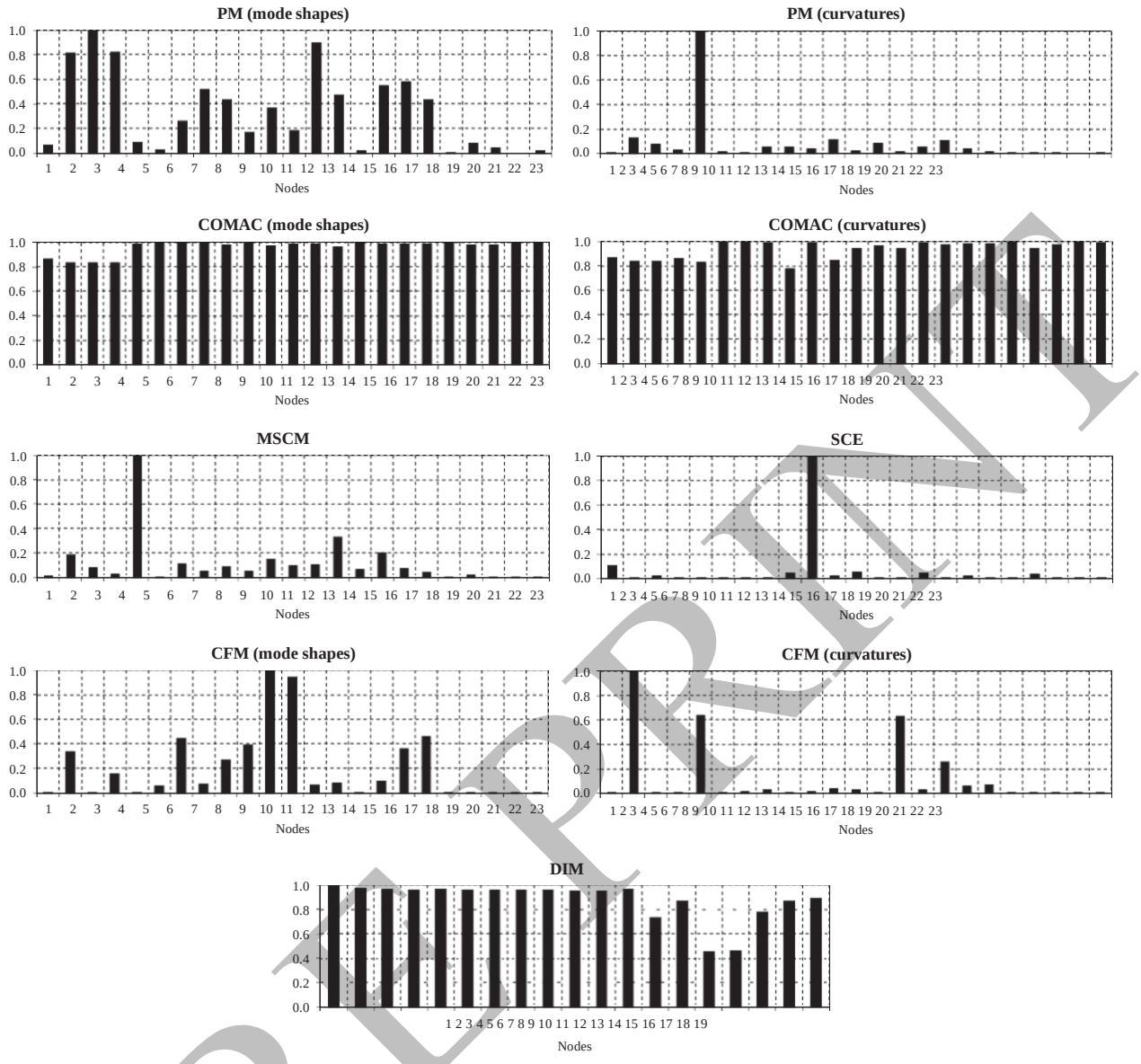

Fig. 14. Damage localization with mode shapes and modal curvatures extracted from impulse data.

has been applied to a numerical model simulating the behavior of the Z24 Bridge. The two structural conditions (undamaged and damaged) needed to put the method into practice are numerically simulated and so are the different inputs used to excite the bridge. Unlike the experimental campaign in which the whole structure was measured in nine set-ups of 33 accelerometers, in this paper the number of channels is reduced to 23, of which 19 points at the deck and 4 points at the piers. The reduction of the number of channels, together with the absence of real excitations, did not allow to achieve an overall dynamic identification of the bridge, but it was enough to catch the meaningful modes of vibration of the structure and to compute the spectral damage index hereby introduced. The results obtained showed a good agreement with the analytical model and allowed to draw the following conclusions:

(1) The spectrum-driven dynamic identification method is a straightforward global technique able to identify the eigenparameters of a structure even using a limited number of sensors;
(2) The method is suitable for output-only techniques as well as for input–output techniques, independently of the excitation source;
(3) The spectral damage index is based on a robust formulation, which is insensitive to user choices, especially with regard to the matrix construction, and it ranges over the whole frequency domain.

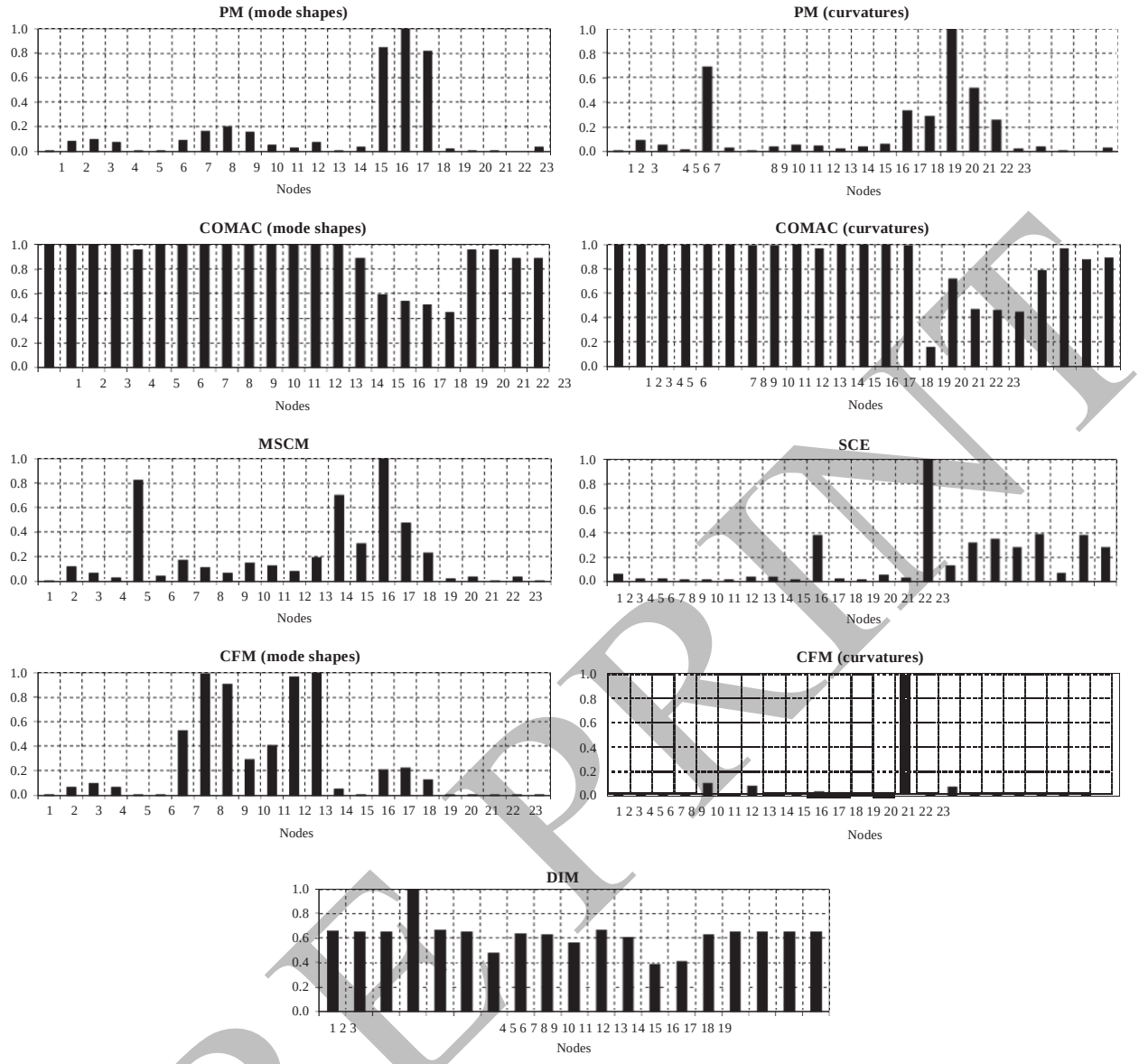

Fig. 15. Damage localization with mode shapes and modal curvatures extracted from shaker data.

The robustness of the spectrum-driven method in damage localization was also highlighted through the comparison with other damage indexes available in the literature. However, it needs to remark that the success of the damage investigation procedure strongly depends on the quality of the output signals. Thus, issues related to optimal sensors selection and location, test planning, acquisition and data processing parameters (e.g. sampling rate, time windowing, filtering, cut-off frequency, etc.) need to be handled carefully. The more accurate the acquisition process, the higher the reliability of the results provided by the spectral damage index. Moreover, attention has to be paid in the selection of the excitation points when dealing with input–output identification techniques as exciting the structure in the proximity of a damaged region can affect the results yielding to false alarm and unrealistic peaks. Yet, the combination of deterministic–stochastic modal analysis techniques can overcome this issue. It is finally stressed that the spectral damage localization index may yield false positives, but it does not yield false negatives which means that the damage is always detected when existing. Notwithstanding, this aspect needs to be further confirmed by examining real data.

In conclusions, the spectral technique hereby presented seems promising and further research is being carried out to address pending issues, such as the definition of a threshold value, the relationship between qualitative and quantitative damage measures, and the performance of the method in noisy conditions. For this latter aspect, in-situ or laboratory experimental activities are preferable.

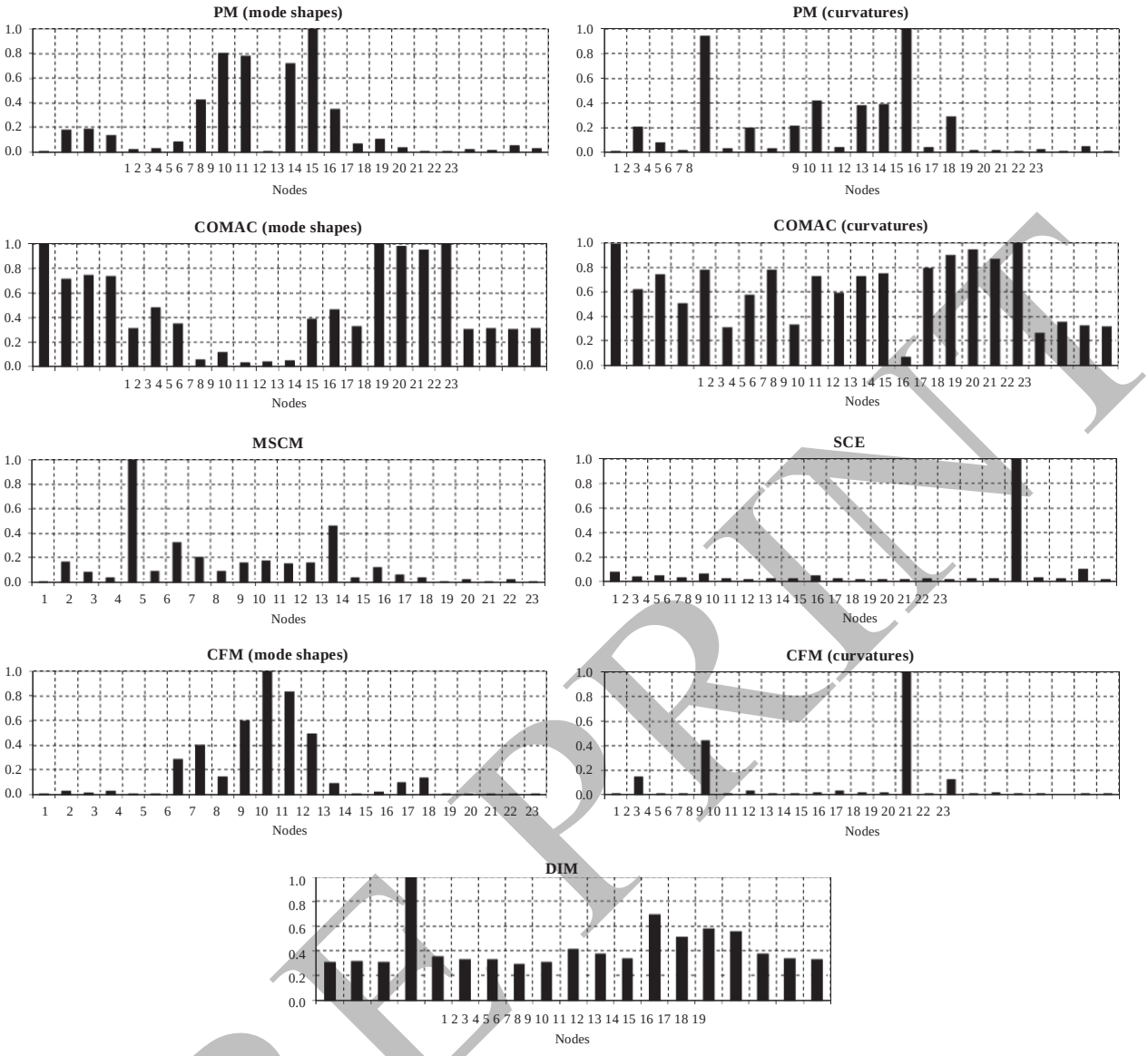

Fig. 16. Damage localization with mode shapes and modal curvatures extracted from random data.

Acknowledgments

The authors would like to express their sincere gratitude to Prof. Dr. Guido De Roeck for sharing his information about the Z24 Bridge. The first author would also like to acknowledge the Italian Ministry of Education, Universities and Research (MIUR) for the Ph.D. scholarship provided.

References

[1] Y.J. Yan, L. Cheng, Z.Y. Wu, L.H. Yam, Development in vibration-based structural damage detection technique, Mech. Syst. Signal Process. 21 (5) (2007) 2198–2211.
[2] S. Doebling, C. Farrar, M. Prime, A summary review of vibration-based damage identification methods, Shock Vib. Dig. 30 (2) (1998) 91–105.
[3] S. Vanlanduit, E. Parloo, B. Cauberghe, P. Guillaume, P. Verboven, A robust singular value decomposition for damage detection under changing operating conditions and structural uncertainties, J. Sound Vib. 284 (3–5) (2005) 1033–1050.
[4] R. Ruotolo, C. Surace, K. Worden, Application of two damage detection techniques to an offshore platform, in: Proceedings of the 17th International Modal Analysis Conference, Orlando, USA, 1999.
[5] A.K. Pandey, M. Biswas, M.M. Samman, Damage detection from changes in curvature mode shapes, J. Sound Vib. 145 (2) (1991) 321–332.
[6] A.K. Pandey, M. Biswas, Damage detection in structures using changes in flexibility, J. Sound Vib. 169 (1) (1994) 3–17.
[7] D. Bernal, Load vectors for damage localization, J. Eng. Mech., 128, , 2002, 7–14.

[8] D. Bernal, B. Gunes, Damage localization in output-only systems: a flexibility based approach, in: Proceedings of the 20th International Modal Analysis Conference, Los Angeles, USA, 2002, pp. 1885–1191.
[9] J.E. Mottershead, M.I. Friswell, Model updating in structural dynamics: a survey, J. Sound Vib. 167 (2) (1993) 347–375.
[10] R. Brincker, P. Andersen, R. Cantieni, Identification and level I damage detection of the Z24 highway bridge, Exp. Tech. 25 (2001) 51–57.
[11] M.G. Masciotta, L.F. Ramos, P.B. Lourenço, M. Vasta, Damage detection on the Z24 Bridge by a spectral-based dynamic identification technique, in: Proceedings of the 32nd International Modal Analysis Conference, Orlando, USA, 2014, vol. 4, pp. 197–206.
[12] A. Rytter, Vibrational based inspection of civil engineering structures, University of Aalborg, Denmark, 1993 (Ph.D. thesis).
[13] K. Worden, J.M. Dulieu-Barton, An overview of intelligent fault detection in systems and structures, Struct. Health Monit. 3 (1) (2004) 85–98.
[14] L.H. Yam, Y.J. Yan, Z. Wei, Vibration-based non-destructive structural damage detection, Key Eng. Mater. 270–273 (2004) 1446–1453.
[15] M. Prevosto, Algorithms d'Identification des Caractéristiques Vibratoires de Structures Mécaniques Complexes, Université de Rennes I, France, 1982.
[16] C.Y. Shih, Y.G. Tsuei, R.J. Allemang, D.L. Brown, Complex mode indication function and its applications to spatial domain parameter estimation, Mech. Syst. Signal Process. 2 (4) (1988) 367–377.
[17] M. Vasta, J.B. Roberts, Stochastic parameter estimation of non-linear systems using only higher order spectra of the measured response, J. Sound Vib. 213 (2) (1998) 201–221.
[18] J.B. Roberts, M. Vasta, Parametric identification of systems with non-Gaussian excitation using measured response spectra, Probab. Eng. Mech. 15 (1) (2000) 59–71.
[19] S. Liberatore, G.P. Carman, J.L. Speyer, Power spectral density (PSD) technique in damage detection, in: Proceedings of SPIE 4327, Smart structures and materials, 2001.
[20] S. Liberatore, G.P. Carman, Power spectral density analysis for damage identification and location, J. Sound Vib. 274 (3–5) (2004) 761–776.
[21] R.K. Giles, B.F. Spencer, Jr., Hierarchical PSD damage detection methods for smart sensor networks, in: Proceedings of SMSST'07, Smart Material and Smart Structures Technology, Chongqing & Nanjing, China, 2007.
[22] S.E. Fang, R. Perera, Power mode shapes for early damage detection in linear structures, J. Sound Vib. 324 (1–2) (2009) 40–56.
[23] K.J. Vamvoudakis-Stefanou, J.S. Sakellariou, S.D. Fassois, Random vibration response-only damage detection for a set of composite beams, in: Proceedings of ISMA, International Conference on Noise and Vibration Engineering, Leuven, Belgium, 2014.
[24] L. Lutes, S. Sarkani, Random Vibrations: Analysis of Structural and Mechanical Systems, Butterworth-Heinemann, MA, USA, 2004.
[25] S. Doebling, C. Farrar, M. Prime, D. Shevitz, Damage Identification and Health Monitoring of Structural and Mechanical Systems from Changes in Their Vibration Characteristics: A Literature Review, Los Alamos National Laboratory, NM, 1996, 132.
[26] E. Carden, P. Fanning, Vibration based condition monitoring: a review, Struct. Health Monit. 3 (4) (2004) 355–377.
[27] H. Sohn, C. Farrar, F. Hemez, A Review of Structural Health Monitoring Literature: 1996–2001, Los Alamos National Laboratory, NM, 2004.
[28] W. Fan, P. Qiao, Vibration-based damage identification methods: a review and comparative study, Struct. Health Monit. 10 (1) (2010) 83–111.
[29] L. Ramos, Damage identification in masonry structures based on vibration signatures, University of Minho, Portugal, 2007 (Ph.D. thesis).
[30] M.G. Masciotta, Damage identification of structures based on spectral output signals, University of Minho (Portugal) & University of "G. d'Annunzio" (Italy), 2015 (Ph.D. thesis).
[31] D.J. Ewins, Modal testing: Theory, Practice and Application, 2nd edition, . Research Studies Press Ltd, 2000.
[32] C. Dong, P.Q. Zhang, W.Q. Feng, T.C. Huang, The sensitivity study of the modal parameters of a cracked beam, in: Proceedings of the 12th International Modal Analysis Conference, pp. 98–104, 1994.
[33] N. Stubbs, J.T. Kim, K. Topole, An efficient and robust algorithm for damage localization in offshore platforms, in: Proceedings of ASCE 10th Structures Congress, pp. 543–546, 1992.
[34] C.B. Moler, Eingenvalues and singular values, in numerical computing with MATLAB, Soc. Ind. Appl. Math. (2004) 269–305. ch. 10.
[35] M. Di Paola, Digital simulation of wind field velocity, J. Wind Eng. Ind. Aerodyn. 74–76 (1998) 91–109.
[36] A. Teughels, G. De Roeck, Structural damage identification of the highway bridge Z24 by FE model updating, J. Sound Vib. 278 (3) (2004) 589–610.
[37] G. De Roeck, B. Peeters, J. Maeck, Dynamic monitoring of civil engineering structures, in: Proceedings of IASS-IACM, Computational Methods for Shell and Spatial Structures, 2000, pp. 1–24.
[38] DIANA, DIANA Finite Elements Analysis - Release 9.4.4, TNO, Netherlands, 2012.
[39] B. Peeters, G. De Roeck, Reference-based stochastic subspace identification for output-only modal analysis, Mech. Syst. Signal Process. 13 (6) (1999) 855–878.
[40] E. Reynders, G. Roeck, Continuous vibration monitoring and progressive damage testing on the Z24 bridge, in: Encyclopedia of Structural Health Monitoring, 2009.
[41] E. Reynders, A. Teughels, G. De Roeck, Finite element model updating and structural damage identification using OMAX data, Mech. Syst. Signal Process. 24 (5) (2010) 1306–1323.